Journal of Hydrology 562 (2018) 84–102

Contents lists available at ScienceDirect

Journal of Hydrology

journal homepage: www.elsevier.com/locate/jhydrol

Research papers

Large scale spatially explicit modeling of blue and green water dynamics in a temperate mid-latitude basin

Liuying Du [a], Adnan Rajib [b], Venkatesh Merwade [a,*]

[a] Lyles School of Civil Engineering, Purdue University, West Lafayette, Indiana, USA
[b] Lyles School of Civil Engineering, Purdue University, West Lafayette, Indiana, USA; now at the Oak Ridge Institute for Science and Education, US Environmental Protection Agency, Office of Research and Development, Cincinnati, Ohio, USA

ARTICLE INFO

Article history:
Received 24 January 2017
Received in revised form 21 December 2017
Accepted 25 February 2018
Available online 17 April 2018
This manuscript was handled by Tim R. McVicar, Editor-in-Chief, with the assistance of Dawen Yang, Associate Editor

Keywords:
Climate change
Land use change
Ohio River Basin
SWAT
Hydrologic modeling

ABSTRACT

Looking only at climate change impacts provides partial information about a changing hydrologic regime. Understanding the spatio-temporal nature of change in hydrologic processes, and the explicit contributions from both climate and land use drivers, holds more practical value for water resources management and policy intervention. This study presents a comprehensive assessment on the spatio-temporal trend of Blue Water (BW) and Green Water (GW) in a 490,000 km^2 temperate mid-latitude basin (Ohio River Basin) over the past 80 years (1935–2014), and from thereon, quantifies the combined as well as relative contributions of climate and land use changes. The Soil and Water Assessment Tool (SWAT) is adopted to simulate hydrologic fluxes. Mann-Kendall and Theil-Sen statistical tests are performed on the modeled outputs to detect respectively the trend and magnitude of changes at three different spatial scales – the entire basin, regional level, and sub-basin level. Despite the overall volumetric increase of both BW and GW in the entire basin, changes in their annual average values during the period of simulation reveal a distinctive spatial pattern. GW has increased significantly in the upper and lower parts of the basin, which can be related to the prominent land use change in those areas. BW has increased significantly only in the lower part, likely being associated with the notable precipitation change there. Furthermore, the simulation under a time-varying climate but constant land use scenario identifies climate change in the Ohio River Basin to be influential on BW, while the impact is relatively nominal on GW; whereas, land use change increases GW remarkably, but is counterproductive on BW. The approach to quantify combined/relative effects of climate and land use change as shown in this study can be replicated to understand BW-GW dynamics in similar large basins around the globe.

© 2018 Elsevier B.V. All rights reserved.

1. Introduction

Under the increasing threats of climate and land use change, fresh water availability will eventually become a limiting resource for many regions across the globe in the near future (Faramarzi et al., 2017). The dynamics of water availability within a region can be analyzed in multiple ways, including statistical methods, sensitivity based methods and distributed hydrologic modeling. Statistical methods mostly involve time-series analysis and non-parametric tests of a particular hydrologic indicator such as streamflow (e.g. Kumar et al., 2009; Sadri et al., 2016; Zhang and Schilling, 2006). A widely used method is the Budyko-based sensitivity analysis framework (Budyko, 1974; Donohue et al., 2011; Jiang et al., 2015; Roderick and Farquhar, 2011; Tan and Gan, 2015; Wang and Tang, 2014; Wang and Hejazi, 2011) to differentiate the role of land use change from that of climate in altering the hydrologic processes. Despite its wide-spread usage, Budyko framework has several conceptual limitations such as the mutual independence of precipitation, evaporation and evapotranspiration, as well as the assumption of steady state water balance with no temporal change in sub-surface storage (Carmona et al., 2016; Greve et al., 2015). Most importantly, use of both the statistical (trend analysis) and the sensitivity (Budyko framework) approaches requires past hydro-climatic data which limits their applicability at required spatio-temporal resolution. In contrast, hydrologic modeling can provide spatially and temporally explicit assessments on surface/sub-surface components by partitioning the water into Blue Water (BW; total water yield and deep aquifer recharge) and Green Water (GW; soil water content and actual evapotranspiration) (e.g. Gerten et al., 2005; Zang et al., 2012).

BW includes the water in rivers, aquifers, and lakes/reservoirs that collectively account for approximately one-third of the total

* Corresponding author at: 550 Stadium Mall Dr., West Lafayette, IN 47907, USA.
E-mail address: vmerwade@purdue.edu (V. Merwade).

https://doi.org/10.1016/j.jhydrol.2018.02.071
0022-1694/© 2018 Elsevier B.V. All rights reserved.

available fresh water; the remaining two-third of the total fresh water is the GW that is stored in the vadose zone and circulates within the water cycle through evapotranspiration (ET) feedbacks (Falkenmark and Rockström, 2006). BW is critical for domestic and industrial water consumption (Döll and Siebert, 2002), whereas GW plays a key role in crop production and other ecosystem services (Zang et al., 2012). Long-term model simulation of BW and GW facilitates identification of *hotspots* that show abrupt temporal change points (e.g. Zang and Liu, 2013) and locations (particular sub-basins) at which water shortage or excess are more likely to occur (e.g. Schuol et al., 2008a,b). Identification of such hotspots is critical for water resources managers/stakeholders where surface or groundwater needs to be abstracted with possible limiting availability without hampering the requirement of the downstream users (Rodrigues et al., 2014). Thus, BW and GW have evolved as the major building blocks for the "water footprint" concept (Hoekstra and Hung, 2002; Hoekstra et al., 2011), which essentially redefine the perception of integrated water resources management by considering not just streamflow at discrete locations but the entire water balance of the basin as "manageable" (Falkenmark and Rockström, 2006). Regardless, long-term spatio-temporal changes in BW-GW in a basin essentially indicate the change in overall hydrologic regime.

With the advent of advanced hydrologic models and computational resources, several large scale modeling studies focusing on BW-GW dynamics exist for a few regions across the globe (Table 1). Most of these studies investigated the role of changing climate on the long-term changes in BW and GW while assuming a constant land use (e.g. Abbaspour et al., 2009; Faramarzi et al., 2009; Schuol et al., 2008a; Zang and Liu, 2013; Zang et al., 2012). Some studies attempted to model BW-GW considering both time-varying climate and land use together (e.g. Liu et al., 2009; Li et al., 2009; Xu, 2013; Zhao et al., 2016). Only a few studies quantified the relative influence of climate and land use on BW-GW dynamics (e.g. Li et al., 2009; Zhao et al., 2016), though for a very limited length of analysis (e.g. 20 years). Unavailability of historical land use data is the main factor that hinders quantifying the relative contribution of climate and land use change. With this inability, their "spatially explicit" correlation with BW and GW could not be deduced in any previous study. Accordingly, calculating the temporal trend or volumetric change in BW-GW without looking into the spatially explicit pattern of climate/land use change masks the hydrologic responses from individual sub-basins (e.g. Li et al., 2009; Xu, 2013). Although such lumped assessments provide insights on how the hydrologic regime is evolving in a particular watershed, these may not be sufficiently helpful in detecting the actual drivers at larger spatial scales. Large scale studies with spatially explicit characterization of climate/land use change impacts are more effective to provide holistic solution at regional and national levels, thereby holding more practical value for future water resources management and policy intervention.

The overall goal of this study is to perform a spatially explicit assessment of changing hydrologic regime, in terms of BW-GW dynamics, in a temperate mid-latitude river basin by:

(i) providing a general evaluation on the historical changes in climate and land use in the past 80 years (1935–2014);
(ii) creating multiple configurations of a large scale hydrologic model that are representative of each decade;
(iii) conducting temporal trend analyses of BW-GW using model simulated outputs at three spatial levels: individual sub-basins, larger sub-regions and the entire basin; and
(iv) quantifying the relative contribution of climate and land use change while relating their respective spatial patterns with BW-GW dynamics.

2. Study area

This study is conducted on the 491,000 km^2 Ohio River Basin (ORB) in the United States, which is the largest tributary of the Mississippi Basin by water volume (Fig. 1). ORB provides a unique test case because land use data for this region are available for past decades from Tayyebi et al. (2015). The elevation in ORB ranges from 30 m above sea level in the flat western parts to 1745 m in the hilly eastern areas. The predominant land use in the western parts of ORB is agriculture due to its flat topography and low elevation, whereas the eastern part is mostly forested. According to the recorded climate data during 1935–2014, annual precipitation for the whole basin ranges from 840 mm/year to 1484 mm/year. The annual average maximum and minimum temperature range from 16.6 to 20.0 °C and 2.5 to 7.3 °C, respectively. The annual precipitation increases slightly from southeast to northwest due to higher elevations in the southeast, while snow accumulation being significant in the north and along the Appalachians in the southeast (White et al., 2005).

The majority portion of ORB lies within the Corn Belt region of the U.S. Midwest, and produces nearly 15–25% of the total corn and soybean in the country (Schnitkey, 2013). In addition to agricul-

Table 1
Comparison of relevant studies evaluating climate and/or land use change impacts on BW-GW.[a]

Reference	BW-GW change assessment		Driver of BW-GW		Relative influence of climate and land use change	Spatially explicit linkage of BW-GW with climate and/or land use change
	Spatial scale	Metric	Climate change	Land use change		
Xu (2013)	Entire basin	Statistical trend test	58 years (1950–2007)	√	×	×
Schuol et al. (2008a)	Regional	Change in volume	25 years (1971–1995)	×	×	×
Abbaspour et al. (2009)	Sub-basin		36 years (1970–2006)	×	×	×
Faramarzi et al. (2009)	Sub-basin		23 years (1980–2002)	×	×	×
Liu et al. (2009)	Sub-basin		42 years (1964–2005)	√	×	×
Zang et al. (2012)	Sub-basin		28 years (1977–2004)	×	×	×
Li et al. (2009)	Entire basin	Statistical trend test + change in volume	20 years (1981–2000)	√	√	×
Zhao et al. (2016)	Sub-basin		20 years (1981–2000)	√	√	×
Zang and Liu (2013)	Sub-basin, regional and the entire basin		60 years (1960–2010)	×	×	×
Du et al. (this study)	Sub-basin, regional and the entire basin	Statistical trend test + change in volume	80 years (1935–2014)	√	√	√

[a] √ indicates "being considered/analyzed in the study", whereas × indicates the opposite.

ture, ORB serves drinking water demand for about 10% of the population and produces about 20% of the electricity for the entire country (America's Watershed Initiative, 2014). Considering the changes in both climate and land use, there is a need to understand how water resources within ORB have been affected in the last several decades. A regional hydro-climatic trend analysis between 1895 and 2011 by the National Oceanic and Atmospheric Administration shows that the average air temperature and annual precipitation in the U.S. Midwest (including ORB) have increased by 0.07 °C and 7.5 mm per decade, respectively (Kunkel et al., 2013). With the increasing population, associated food demand and rising grain prices, conversion of native grassland to agricultural areas has been the primary land use change in the Midwest/Great Plains states after mid 20th century (Paul et al., 2017; Sleeter et al., 2013). However, ORB has experienced a unique land transformation from agriculture to forest since 1950s, mainly due to the Agricultural Act of 1956 and Conservation Reserve Program of 1985 (Lytle, 2010; USFS, 2009; USDA, 2015). These conservation policies encouraged farmers to convert erodible or environmentally sensitive croplands into forests. With the enactment of a more recent public policy – Energy Independence and Security Act of 2007), there has been another paradigm-shift in ORB's land use practice as the farmers have started growing biofuel pastures on degraded, marginally suitable lands (Drummond et al., 2012; Rajib et al., 2016a;

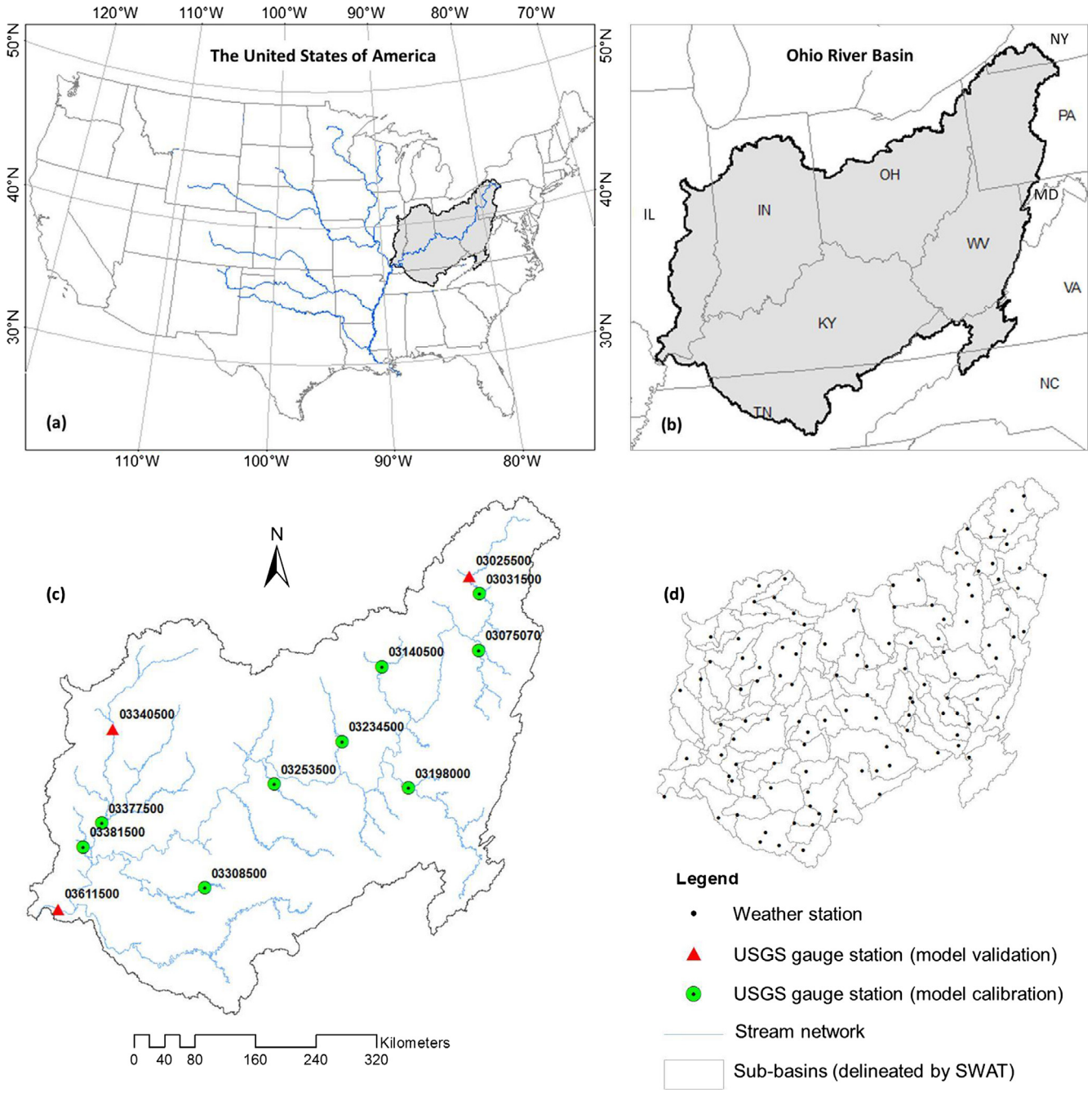

Fig. 1. (a) Location of the Ohio River Basin (ORB) in United States along with the schematic flowline of the Mississippi River System; (b) the 11 states comprising ORB drainage area (IL: Illinois, IN: Indiana, OH: Ohio, NY: New York, PA: Pennsylvania, MD: Maryland, TN: Tennessee, KY: Kentucky, WV: West Virginia, VA: Virginia, NC: North Carolina); (c) United States Geological Survey's streamflow gauge stations selected as model calibration and validation locations (numbers correspond to respective USGS station IDs); (d) Sub-basins delineated by the Soil and Water Assessment Tool (SWAT) and the weather stations providing precipitation and temperature data in this study.

Schilling et al., 2008; Sohl et al., 2014; Sohl et al., 2012). The population is also continuously growing in the Midwestern states, with an average annual growth rate of 3.8% during 2000–2009 (Eathington, 2010), giving way to increasing urbanization. Against this background, an improved understanding of the combined and the relative role of climate and land use changes will afford effective management of current and future water resources in this region.

3. Methods

3.1. Evaluating historical changes in climate and land use (1935–2014)

Representative land use data for the past 80 years (1935–2014) are analyzed to determine a temporal pattern of interchanges among different land use classes. Sub-basins experiencing land use change are identified through GIS processing such that the "dominant" land use within a sub-basin got shifted from one type to another. Statistical trend analyses are performed using the basin-average annual precipitation, air temperature and potential evapotranspiration (PET) data, enabling the identification of a relatively prominent indicator of climate change.

3.2. Creating multiple configurations of a large scale hydrologic model for each decade

Hydrologic simulation to evaluate the combined and relative influence of climate and land use change on BW-GW is performed by the Soil and Water Assessment Tool (SWAT; Arnold et al., 2012; Neitsch et al., 2011). SWAT is chosen because it is extensively tested in large spatial scales under different geophysical settings (e.g. Abbaspour et al., 2015; Faramarzi et al., 2017; Rajib and Merwade, 2017; Schuol et al., 2008a; Zang et al., 2012); accordingly, similar modeling approach such as the one presented here can be replicated for other large basins across the globe.

3.2.1. Input data

The topography data for SWAT modeling is obtained from US Geological Survey's (USGS) 30 m resolution National Elevation Dataset (USGS-NED, 2015). The 1:250,000 scale State Soil Geographic Data (STATSGO) is included from the model's built-in database. Five historical land use data sets, one for each decade during 1935–1985, are obtained from the Human-Environment Modeling and Analysis Laboratory, Department of Forestry and Natural Resource at the Purdue University (Tayyebi et al., 2015). These land use maps feature four major land cover classes: forest and rangeland, agriculture, urban and others (e.g. wetland/barren). For the remaining three decades of the study period (1985–2014), land use maps are obtained from multi-year USGS National Land Cover Database (1992, 2001 and 2011) (USGS-NLCD, 2016). The original NLCD maps are reclassified into the same generic classes as in the historical land use maps for 1935–1985 to reduce uncertainty that might have evolved from dissimilar techniques used in generating the datasets.

The climate data are obtained from 112 National Climatic Data Center (NCDC) weather stations (Fig. 1) which are uniformly distributed within the basin, and have continuous records. These stations provide total daily precipitation, average daily maximum and minimum temperature covering the entire period of simulation. NCDC maintains a nationally recognized database that goes through standard quality-checks, so no prior statistical tests are performed on the climate data. All other relevant data, such as solar radiation, wind speed and relative humidity, are created through the internal weather generator in SWAT. Observed daily streamflow time series for model calibration and validation are obtained from selected USGS gauge stations (Fig. 1).

3.2.2. Model configurations

Nine SWAT models, divided under two different configurations, are developed to evaluate the combined and individual impacts of climate and land use on BW-GW. The first model configuration incorporates the combined effect of climate and land use for which the entire 80 year study period (1935–2014) is divided into 10-year segments; eight SWAT models are created – one separate model for each decade by using the corresponding representative land use and climate data. In the second model configuration, the impacts of climate and land use are isolated by creating a single SWAT model based on the 1940s land use and historical climate data over the same 80 year span. In simple terms, the first model configuration involves variable land use and variable climate, and the second configuration involves constant land use and variable climate. The spatial heterogeneity is represented in the models by dividing ORB into 125 sub-basins using 2500 km^2 as the threshold area for stream network delineation. To reduce computational burden, all geospatial datasets are processed at 90 m spatial resolution. Similarly, a single Hydrologic Response Unit (HRU) is created for each sub-basin based on the "dominant" land use, soil type and slope class following several other SWAT applications (Faramarzi et al., 2017; Ndomba et al., 2008; Oeurng et al., 2011; Schuol et al., 2008a,b; Tibebe and Bewket, 2011). Considering the elevation difference across the basin, slope is divided into three classes (0–4%, 4–10%, and >10%). Because the changes in BW-GW will be eventually quantified at a sub-basin scale, it is assumed that single HRU sub-basins will produce reasonable results. To validate this assumption, a prototype SWAT model was created for the 'variable climate – variable land use' configuration with 10% area-aggregation threshold for soil, slope and land use to generate 1670 HRUs for the 125 sub-basins. Although the daily simulated outputs from this porotype model were not identical as in the "dominant" model setup, the aggregated annual sub-basin averages of the BW-GW components did not show any noticeable difference. This is analogous to the findings by Her et al. (2015) as well.

Penman-Monteith equation is selected for computing PET, and the hydrologic processes related to surface runoff generation and channel routing are simulated using the Curve Number and Variable Storage methods (Neitsch et al., 2011), respectively. Nearly 30% of ORB has artificial subsurface drainage (tile drainage) (Sugg, 2007), a big portion of which was installed before 1960s (Zucker and Brown, 1998). Due to the absence of a database listing the actual spatial coverage of subsurface drainage, their depth, spacing and actual date of installation, all the sub-basins having 'poorly-drained' and 'very poorly-drained' soil are simulated by using the tile drainage routine in SWAT (e.g. Boles et al., 2015; Boles, 2013; Du et al., 2005; Green et al., 2006). In SWAT, four major parameters, DEP_IMP (depth to impermeable layer, mm), DDRAIN (depth to drain, mm), TDRAIN (time to drain soil to field capacity, hr) and GDRAIN (drain tile lag time, hr) are responsible in simulating flow through the tile drains (Neitsch et al., 2011). Here, values for these four parameters are set to 1200 mm, 1000 mm, 24 h and 48 h, respectively, following previous studies on several agricultural watersheds within ORB (e.g. Boles et al., 2015; Boles, 2013; Kladivko et al., 1991; Larose et al., 2007).

3.2.3. Model calibration and validation

For the first modeling configuration to study the combined impact of land use and climate change on BW-GW, SWAT model is calibrated for each decade by using daily streamflow observations from nine USGS gauge stations (Fig. 1). The calibration stations are selected based on data availability along the 80 year

span as well as the uniform distribution of station locations across the basin. As recommended by Daggupati et al. (2015a), the last three years from the previous decade are used as initialization/warm-up period in every case. After obtaining the best estimates (most optimal) of the parameters from calibration, models are cross-validated for each decade by using three different USGS gauge stations that are not included in the calibration phase (Fig. 1). The validation stations are chosen to capture the varied topography and land use in the basin. The above mentioned setup results into eight sets of calibrated parameters, one for each decade, for the first model configuration. For the second configuration which isolates the impact of land use, the model is calibrated for 75 years (1935–2014) with a 5 year warm-up period (1935–1939) by using the same calibration and validation stations as in the first model configuration.

A total of 18 parameters involving surface, subsurface and channel hydrologic responses are used for calibration (Table A.1 in Appendix A). The selection of parameters and their initial ranges are based on the review of existing literature and prior knowledge of the U.S. Midwestern watersheds (e.g. Ahiablame et al., 2017; Rajib and Merwade, 2017), as well as suggestions from model developers (Neitsch et al., 2011). Calibration is conducted using the Sequential Uncertainty Fitting alogorithm-version2 (SUFI-2), which is a semi-automated inverse modeling procedure available inside SWAT-CUP (Abbaspour, 2015). Kling-Gupta Efficiency (KGE) (Gupta et al., 2009; Kling et al., 2012) is used as the goal/objective function to measure the association between simulated and observed streamflow hydrographs. In this multi-objective parameter optimization, the best estimates of the parameters are sought through an aggregated value of the goal (KGE′, Eq. (1)) following the approach of Rajib et al. (2016b):

$$KGE' = \sum_{i=1}^{n} w_i (KGE_i) \tag{1}$$

where i denotes the streamflow gauge stations brought under calibration and w is the weight assigned to each of them; n is the total number of gauge stations involved (observational datasets). Here, equal weights are assigned to every gauge station ($w_i = 1/n$). Thus, KGE calculated for individual sets of observed and simulated streamflow hydrographs are aggregated into KGE′ and it is maximized towards an optimal solution. After calibration and validation, both model configurations are re-run for 1935–2014 by using the respective calibrated parameter set(s) to obtain continuous output over the 80 year time span. All the change assessments on BW-GW performed in this study are based on average annual model outputs which are aggregated from the calibrated daily simulations.

3.3. Conducting temporal trend analyses of BW-GW using model simulated outputs

The Mann-Kendall (MK; Mann, 1945; Kendall, 1948) test is used to detect the monotonic trends in annual precipitation, temperature, PET, BW and GW. MK is a rank based, nonparametric trend test that does not require the data to follow a specific statistical distribution. However, hydroclimatic time series often have significant serial correlations (auto-correlations) which can affect the accuracy of MK results, that is, positive serial correlation in a time series increases the probability for MK to detect a significant trend (von Storch, 1999; Yue et al., 2002). An autocorrelation test on BW and GW indicated that the influence of serial correlation in the data can be neglected in this study (Fig. B.1 in Appendix B). The MK rank correlation coefficient, tau (τ), is calculated to determine whether the trend is increasing ($\tau > 0$), decreasing ($\tau < 0$) or not changing ($\tau \sim 0$). Three significance levels are classified based on the p-values: not significant (NS; $p > 0.1$), significant (S; $0.1 > p > 0.01$) and very significant (VS; $p < 0.01$). Following MK test, slope of the trend is calculated using Theil-Sen approach (TS; Sen, 1968). The slope determined by TS is the estimator of change magnitude.

3.4. Quantifying the relative contribution of climate and land use change

The relative effects of climate and land use changes on BW and GW are quantified using an approach similar to the one applied by Guo et al. (2016), Li et al. (2015), Li et al. (2014) and Li et al. (2012). Application of this approach involves the following two assumptions: (i) climate and land use changes are the sole factors affecting the spatio-temporal trend of BW-GW, and (ii) impacts of climate and land use change on BW and GW are independent. To be consistent with these assumptions, the two model configurations must be mutually exclusive. Not calibrating the second configuration (variable climate-steady land use), rather constructing it simply based on the calibrated parameters of the first configuration (variable climate-variable land use) would make the second fully dependent on the first, turning the above assumptions invalid.

Based on the outputs from the first model configuration involving 'variable climate-variable land use', the difference in annual values of BW and GW between two discrete time periods can be expressed by equations (2) and (3),

$$\Delta BW = BW_{2014} - BW_{1935} \tag{2}$$

$$\Delta GW = GW_{2014} - GW_{1935} \tag{3}$$

where subscripts 1935 and 2014 represent the annual values for BW and GW given by the TS trend line corresponding to the initial (1935) and final (2014) year of comparison. ΔBW and ΔGW are the respective differences between 1935 and 2014 in response to both climate and land use changes (first model configuration). Likewise, equations (4) and (5) can be used with outputs from the second model configuration (variable climate-steady land use), to obtain the change in annual BW and GW resulted from climate change only (ΔBW_C and ΔGW_C).

$$\Delta BW_C = BW'_{2014} - BW'_{1935} \tag{4}$$

$$\Delta GW_C = GW'_{2014} - GW'_{1935} \tag{5}$$

where BW' and GW' represent the corresponding annual BW and GW values given by the TS trend line under the second configuration. By subtracting the second configuration (equations (4) and (5)) from the first one (equations (2) and (3)), change in BW and GW due to land use change (ΔBW_L and ΔGW_L) can be obtained as the following:

$$\Delta BW_L = \Delta BW - \Delta BW_C \tag{6}$$

$$\Delta GW_L = \Delta GW - \Delta GW_C \tag{7}$$

Then, the 'Change Ratios' are defined representing the relative effect of climate and land use changes as described by equations (8) and (9).

$$bw_C = \Delta BW_C/\Delta BW, \text{ and } bw_L = \Delta BW_L/\Delta BW \tag{8}$$

$$gw_C = \Delta GW_C/\Delta GW, \quad \text{and } gw_L = \Delta GW_L/\Delta GW \tag{9}$$

where bw_C (gw_C) and bw_L (gw_L) give the relative effect on blue water (green water) due to climate and land use change, respectively.

4. Results

In this section, a general assessment of climate and land use change in ORB is first presented based on past climate records and land use databases during the 80 year study period (1935–2014). After the evaluation of calibrated model performances against observed streamflow data, trend of changes in BW and GW from the first modeling configuration (variable climate-variable land use) are presented at the sub-basin, regional and basin level. Finally, the relative contribution of climate and land use change on BW and GW is evaluated based on the second modeling configuration (variable climate-steady land use).

The dominant land use in ORB during 1940s was agriculture, covering 55% of the total basin area, while forest and urban area constituted 35% and 7%, respectively (Fig. 2). In the following decades, both forest and urban land uses increased by partially replacing agricultural areas. The forest cover has significantly increased in the upper region, more specifically the northeast part of the basin. By 2010, forest and urban areas were covering 51% and 10% of the total basin area, respectively, thereby reducing the agricultural land use from 55% to 37%. The increase in urban area by 3% was much less compared to the change in forest area, which increased by 16%.

Based on the MK-TS test results, annual precipitation increased by 78 mm in 2014, which is about 8% higher than the precipitation in 1935 (Fig. 3). Nevertheless, prominent fluctuations from the trend line (Fig. 3(a)) throughout the study period are indicative of persistent climate variability in ORB. Fig. 3(b) shows a statistically insignificant decreasing trend of PET across ORB. In this case, PET is calculated with SWAT's built-in Penman-Monteith equation (Neitsch et al., 2011) using all the relevant energy-related weather inputs including air temperature, solar radiation, wind speed and relative humidity. Annual maximum temperature dropped by 1 °C and the annual minimum temperature increased by 0.4 °C, indicating a trend of 'cooler days' and 'warmer nights' (Fig. 3(c)). As a result of the opposing trends in the maximum and minimum temperature, no clear trend is visible in average temperature. It is well-accepted that the statistical trend of a hydro-climatologic time-series depends on the length of data that is included in the test. Looking only at a specific span of time may create a different impression contrary to what would have been identified from a much longer time-series. From this aspect, using 80 years of data is rather indicative of the analytical strength to capture hydrologic changes more realistically, contrary to the previous studies that are based on much shorter time-spans (Table 1).

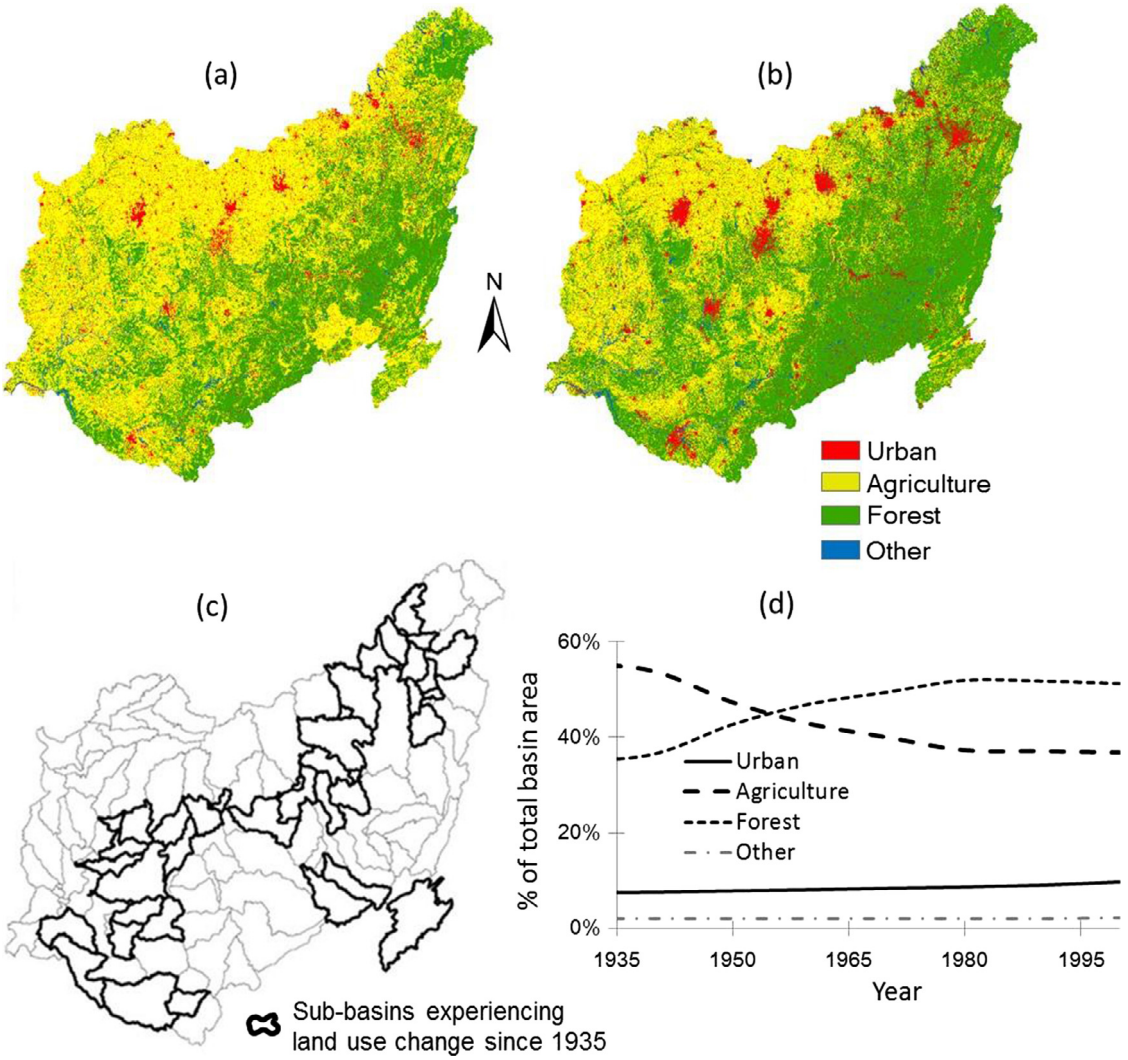

Fig. 2. (a) Representative land use for 1935–1944 (Tayyebi et al., 2015); (b) representative land use for 2005–2014 (National Land Cover Database 2011); (c) sub-basins (dark boundary) experiencing land use change during 1935–2014 such that "dominant" land use within a sub-basin got shifted from one type to another; (d) intercomparison of different land use classes expressed as the percentage of total basin area.

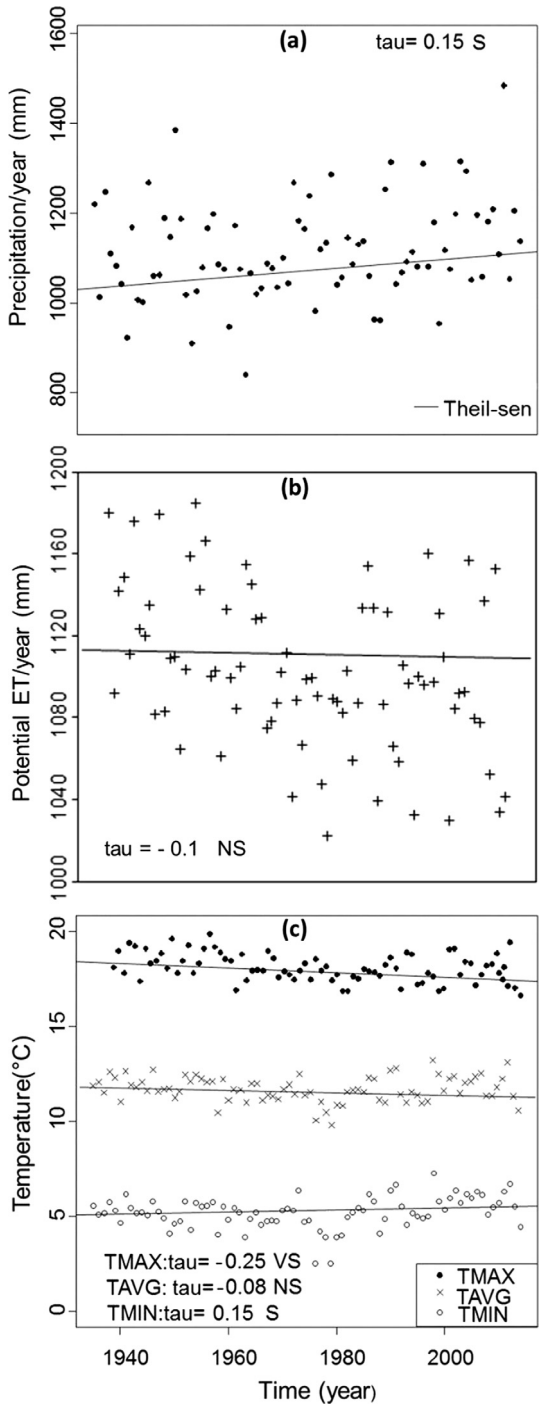

Fig. 3. Mann-Kendall (MK) trend analysis on (a) precipitation, (b) potential ET, and (c) maximum, average and minimum temperature. Note: tau (τ) is the rank correlation coefficient, where tau > 0 indicates an increasing trend and vice versa; "NS": not significant in MK test, "S": statistically significant at $p < 0.1$; "VS": very significant at $p < 0.01$ (Section 3.3).

Fig. 4 shows the change in annual precipitation in each sub-basin by comparing the annual average in 1985–2014 to that in 1935–1964. In general, precipitation has increased remarkably in majority of the sub-basins, which is analogous to the findings shown in Fig. 3(a). Increased precipitation amount is observed mostly in the northeast and northwest parts, while a slight decrease is noticeable in the middle and southern parts. Current version of SWAT assigns the nearest climate station to each sub-basin (not an interpolation). Because the calculated change in precipitation is representative of an entire sub-basin, there can be abrupt differences in the change values among adjacent sub-basins. Based on the spatial characterization of sub-basin scale land use and precipitation changes, the entire basin can be divided into three regions: the upper region (upstream), middle region, and lower region (downstream). Accordingly, Fig. 4 shows sub-basins that have experienced change either in land use or precipitation or both. The quantitative assessment of precipitation and land use change in ORB as shown in Table 2 validates the rationale for aforementioned regional sub-divisions.

To ascertain that the calibrated SWAT models are representative of ORB's geophysical characteristics, simulated daily streamflow at three validation locations (Fig. 1) are compared with USGS gauge data for the 80 year simulation period (Fig. 5). It should be noted that the hydrographs presented in Fig. 5 correspond to the variable climate-variable land use configuration, asserting the credibility of the models to capture climate and land use change impacts. The goodness of fit scores (KGE, Nash-Sutcliffe Efficiency (NSE) and Percent Bias (PBIAS, expressed in % units) for both model configurations (variable/steady land use) are summarized in Table 3, separately for the calibration and validation phases. Regardless of calibration or validation, KGE and NSE in daily simulation range from 0.38 to 0.85 with PBIAS from −20% to +1%. Fig. 6 shows the goodness of the model in terms of seasonal and annual variability in streamflow, where simulated average annual streamflow is found to have KGE ranging from 0.69 to 0.82 in all the three validation locations. Table A.2 (Appendix A) reports the optimized parameter values (best estimates). Assessments of trends in BW-GW are performed based on average annual SWAT outputs.

Figs. 7 and 8 shows trend analyses results for BW-GW for each of the 125 sub-basins, featuring the combined effects of climate and land use. Such spatially explicit assessment helps to relate changes in BW-GW with their corresponding driving factors at the sub-basin level. Fig. 9 presents the trend results for the three regions separately (upper, middle and lower), while Fig. 10 shows the same when analyzed at the entire basin scale. Significant or very significant increases in both BW and GW trends are found in the lower region. For the basin as a whole, the amount of both BW and GW has increased during the study period, however, with different levels of statistical significance. Results from the TS test as summarized in Table 4 show a basin-average increase in BW by 35.5 mm, although the trend of change (MK test) is found insignificant ($p > 0.1$). As estimated by the TS trend line, basin-average GW has changed very significantly ($p < 0.01$) with an increase of 64.5 mm in 2014 compared to that in 1935.

5. Discussion

5.1. Characterizing historical changes in land use and climate

Any sub-basin in ORB experiencing change of land use such that the past "dominant" land use therein got shifted to another type is identified in Fig. 2(c) (and also in Fig. 4). Although Fig. 2(d) shows a basin-level generic trend in ORB with agricultural areas being converted into forest and urban areas, that trend has all but ceased since the last two decades (Lytle, 2010). Accordingly, there is evidence of continuous agricultural intensification in the lower (downstream) region, especially due to growing interests for producing biofuel pastures in marginal lands (e.g. Rajib et al., 2016a). Overall, one-third of ORB experienced noticeable land use change over a span of 80 years, most of which occurred in the northeast and southwest regions. These temporal changes in land use practices are crucial for capturing BW-GW dynamics more realistically, which is not possible by considering only climate

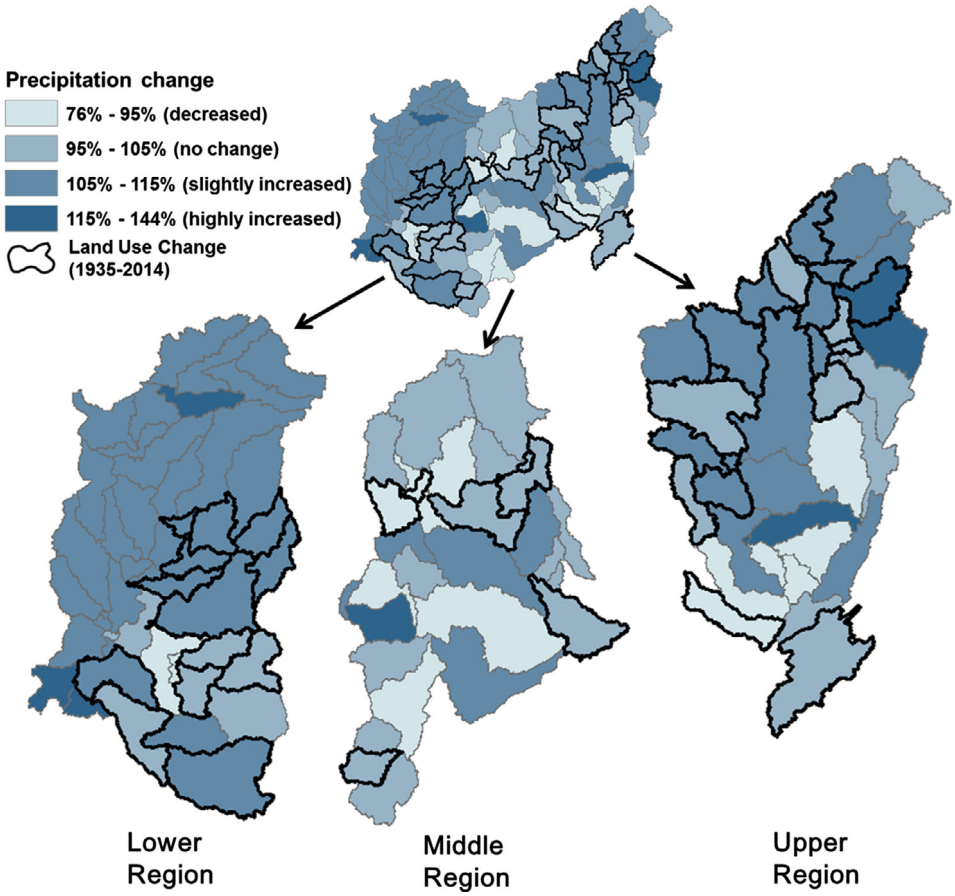

Fig. 4. Sub-division of Ohio River Basin into three regions according to the climate (precipitation) and land use (Fig. 2) change pattern. Change values correspond to the calculated "change ratio" between the 30 year average annual precipitation during 1985–2014 and 1935–1964.

Table 2
Regional comparison of precipitation and land use change in Ohio River Basin during 1935–2014. Values indicate percentage area within the respective regions.

		Upper region (upstream)	Middle region	Lower region (downstream)
Land use change[a]		41	15	35
Precipitation change[b,c]	Decreased	15	29	3
	No change	30	49	15
	Slightly increased	46	19	78
	Highly increased	9	3	4

[a] Based on "dominant" change in land use per sub-basin (example: agriculture transforming into forest or vice versa). Caption of Fig. 2 explains the meaning of "dominant" change.
[b] Change is indicated by the ratio of average annual precipitation during the recent 30 year (1985–2014) and the past 30 year of the study period (1935–1964).
[c] Values within one particular region sum up to 100%.

change in the hydrologic simulation. Because of the relatively small increase in urban areas compared to other land uses, it is assumed that the effect of urbanization on basin-scale hydrology is nominal.

Increasing annual precipitation in ORB indicates more availability of water albeit inter-annual variability (Fig. 3(a)). While precipitation is the supply of water, potential evapotranspiration (PET) is the index of "available energy" that drives water back to atmosphere. Several studies have shown altered trends of solar radiation (Wild, 2009), vapor pressure (Willett et al., 2008) and wind speed (McVicar et al., 2012) in different parts of the globe, which are the key determinants of PET in addition to just air temperature. Therefore, looking only into temperature might not provide a holistic perspective on the changing trend of atmospheric evaporative demand (Donohue et al., 2010), hence, the whole water balance (Donohue et al., 2011; Liu and McVicar, 2012). For ORB, a declining trend of PET is detected in Fig. 3(b), which is supported by the declining wind speed observed in past several decades in the U.S. Midwest (Pryor et al., 2009), and also by the invariant average temperature trend in Fig. 3(c). These results are often specific to the period of study, which may be different from what could have been observed in a longer duration trend analysis. For example, Rogers (2013) showed a cooling trend of average annual temperature (~−0.5 °C/century) in the most parts of ORB during 1895–2007. Karl et al. (1996) found the same over the period of 1900–1994. Under the particular context of this study, absence of noteworthy trends in average temperature and PET but a significant increasing trend of precipitation suggests that precipitation is the primary indicator of climate change in ORB.

It is important to detect a characteristic spatial pattern of precipitation and land use changes across the basin so that a coherence can be established with the corresponding changes in BW-GW, both qualitatively and quantitatively. The regional subdivisions presented in Fig. 4 are derived solely from such perspec-

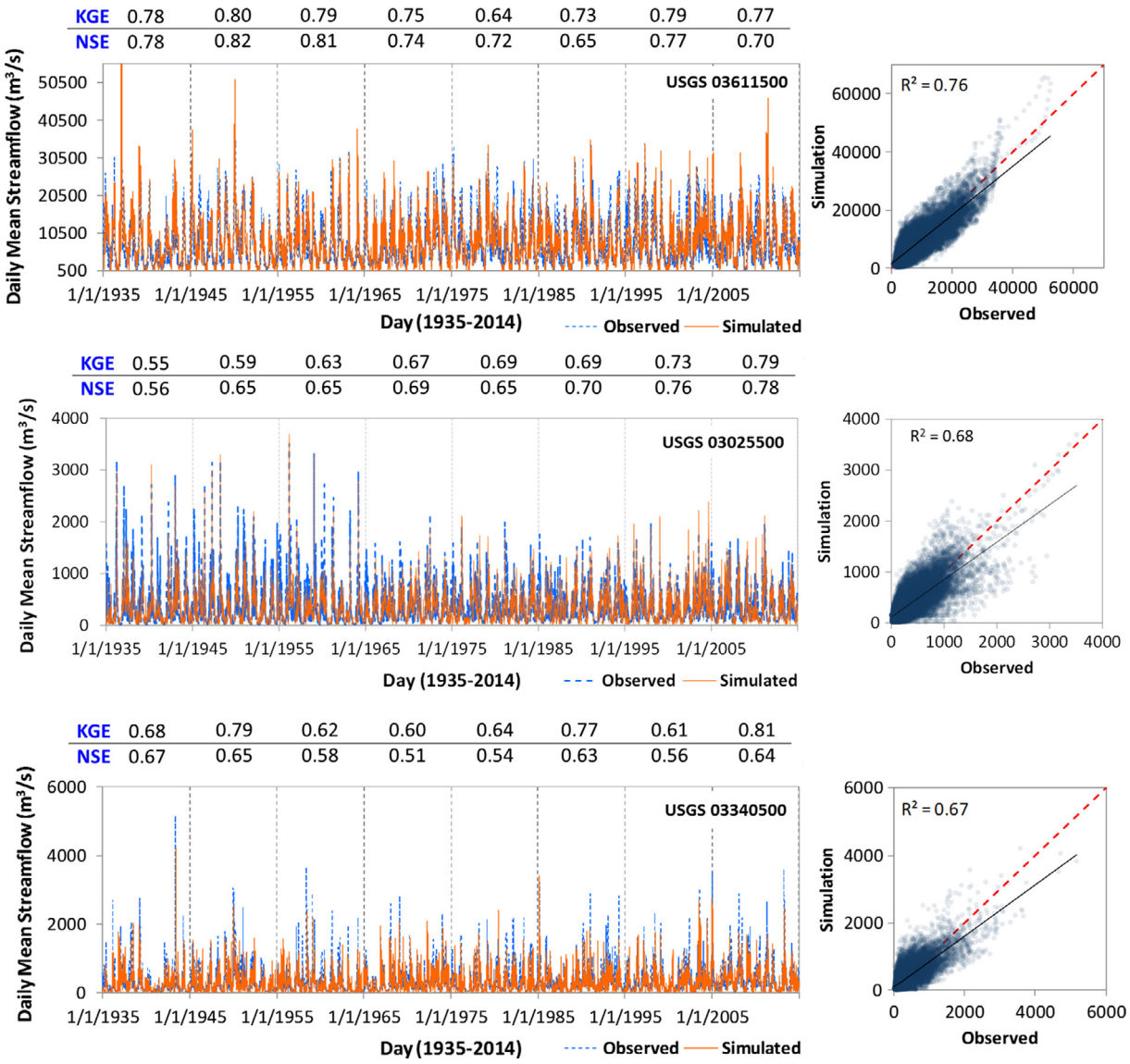

Fig. 5. Model validation: simulated daily streamflow hydrograph from the 'variable climate-variable land use' model configuration is compared here with the corresponding observed data.

Table 3
Streamflow prediction skills during calibration and validation periods, based on simulations at daily time-step.[a]

	Variable climate – variable land use[b]			Variable climate - steady land use[c]		
	KGE	NSE	PBIAS (%)	KGE	NSE	PBIAS (%)
Calibration locations						
03031500	0.64	0.67	−16	0.68	0.72	−8
03075070	0.56	0.55	−12	0.57	0.56	−1
03140500	0.72	0.63	−6	0.62	0.51	15
03198000	0.54	0.51	−9	0.61	0.60	2
03234500	0.71	0.50	8	0.43	0.45	18
03253500	0.49	0.39	3	0.46	0.38	5
03308500	0.54	0.47	−16	0.41	0.42	−20
03377500	0.86	0.79	1	0.68	0.71	9
03381500	0.68	0.69	4	0.54	0.55	10
Validation locations						
03340500	0.69	0.61	−6	0.61	0.57	7
03025500	0.54	0.49	−15	0.66	0.60	−12
03611500	0.75	0.76	−8	0.69	0.70	9

[a] Fig. 1 shows the locations of these stations within the basin, with respective ID numbers.
[b] Values correspond to average statistics from all the 8 SWAT models within this configuration. Each of the models is calibrated/validated separately for its respective 10 year simulation period.
[c] A single SWAT model for the entire 80 year study period (1935–2014) considering a steady land use since 1940s.

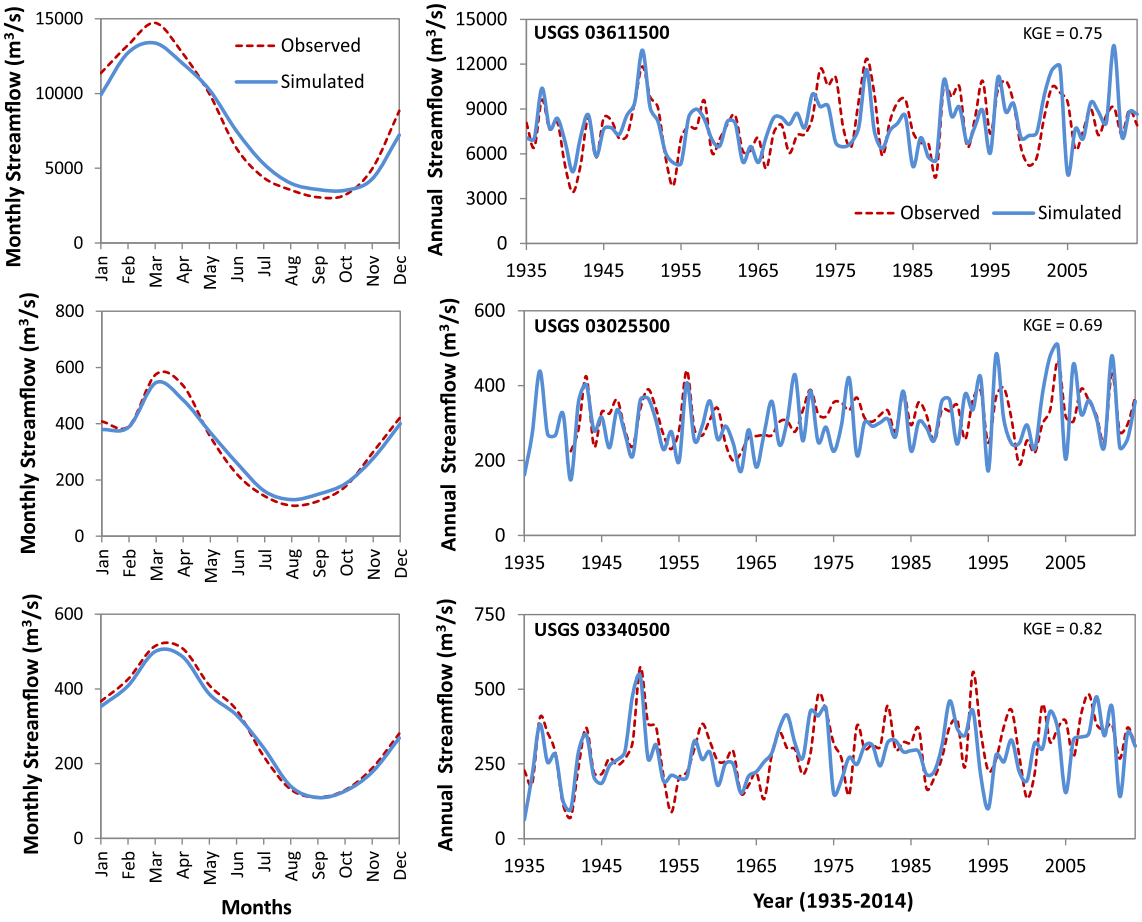

Fig. 6. Model validation for the 'variable climate-variable land use' configuration. (Left) seasonal variability of streamflow. Value in a particular month (e.g. May) is the average of all the monthly mean May streamflow values during 1935–2014. (Right) annual mean streamflow hydrographs.

tive. In general, land use change in both upper and lower regions of ORB is substantial, while the precipitation increase in the lower region is relatively greater than that in the upper region. Changes in land use and precipitation in the middle region are not as extensive as they are in the other two regions (Table 2).

5.2. Model evaluation

Reasonably good agreement with the observed streamflow data at seasonal and annual time-scale, as revealed by Fig. 6, shows the efficacy of simulated BW-GW components to realistically capture the hydrologic responses. All BW-GW components are calculated here using the annual outputs that are originally simulated at daily time-scale. Despite being computationally intensive, daily calibration is preferred over monthly or annual calibration with an expectation of better constraining the model.

The calibrated daily streamflow hydrographs from SWAT match well with the observed data, except for several high flow events. This is analogous to findings from many past studies across different regions that report deficiency of the SWAT model in simulating extreme flow conditions (e.g. Daggupati et al., 2016; Rajib and Merwade, 2016). Performance measures in the variable climate-variable land use configuration are relatively better than the variable climate-steady land use configuration for most of the stations (Table 3), thus demonstrating the effect of using representative land use in the model for each decade. Relatively higher PBIAS values in some locations can be partly attributed to the insufficient representation of precipitation dynamics in certain portions of ORB. The 112 weather stations, though uniformly distributed over the 490,000 km^2 basin area, provide only one point-input approximately for each 4500 km^2. Advanced remotely sensed gridded precipitation estimates are not suitable for this study because of their issues related to relatively short period of data availability and possible uncertainty compared to ground observations (Price et al., 2014). Regardless of the variable/constant land use configurations or calibration/validation, persistence of apparently systematic (and noticeably higher) PBIAS in the forested region (Table 3) is most likely caused by the assumption of constant surface/canopy resistance in PET calculation (Milly and Dunne, 2016). Use of a coarse resolution DEM (90 m) could also be a factor in this case given the fact that much of the mid-basin and upstream forested region of ORB has high topographic variability. These cause-and-effect evaluations are detectable from Fig. 5, where the simulated daily streamflow hydrograph in a validation location (USGS 03025500; forested region with high topographic relief) is prominently underperforming compared to another location (USGS 03340500) representing flat agricultural landscape. An obvious reason for large variability in PBIAS estimates, across the basin or between two model configurations at the same station, could be the sub-optimality in "streamflow-only" calibrations. This problem can be addressed through a multi-variable spatially distributed calibration scheme (e.g. Kunnath-Poovakka et al., 2016; Rajib et al., 2016b). Regardless, a high PBIAS value in a daily calibration can be significantly influenced by the biases in few events (e.g. model not capturing the extreme peak flows) even though the model performance is generally good. Overall, the calibrated SWAT models developed in this study are able to reasonably capture the time response and total volume of fluxes, with slight deficiency in some

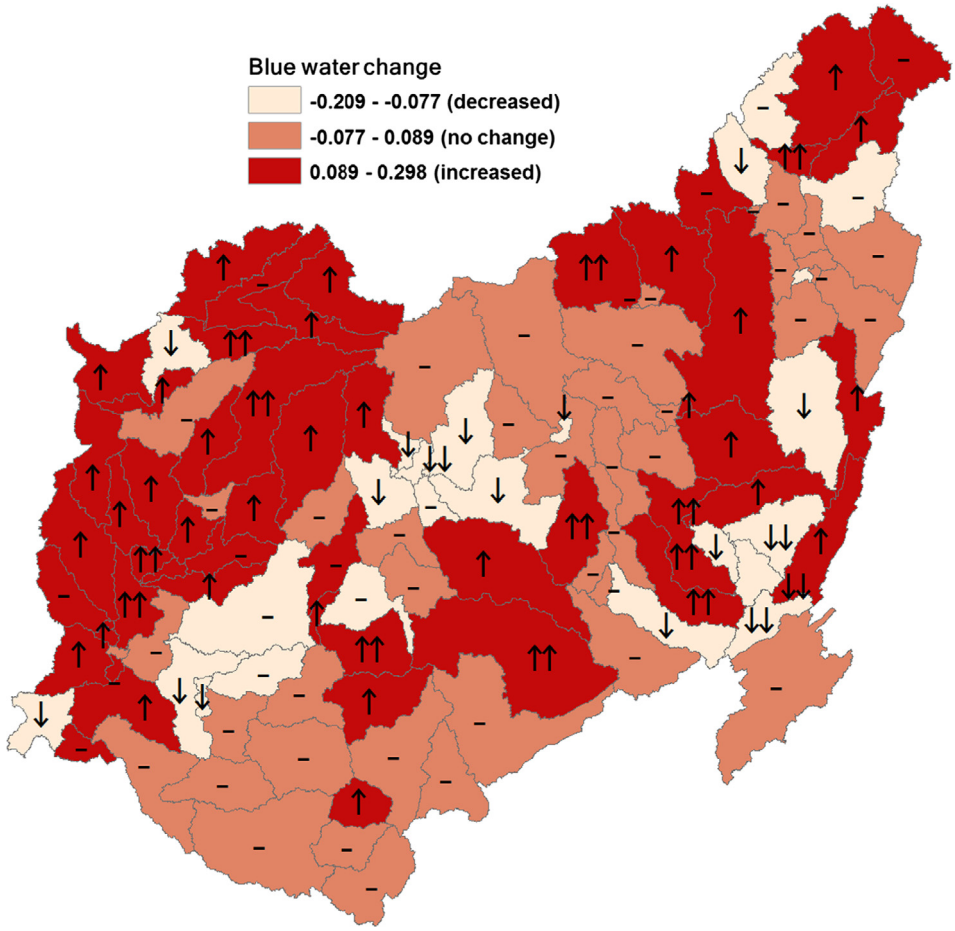

Fig. 7. Sub-basin scale MK trend analysis on blue water (BW). Colors represent the decreasing or increasing trends where higher intensity indicates higher tau (τ) value: increasing (τ > 0), decreasing (τ < 0) or not changing (τ ~ 0). Arrows represent the significance level. "–": trend not significant, "↑": significant increase ($p < 0.1$), "↑↑": very significant increase ($p < 0.01$), "↓": significant decrease ($p < 0.1$), and "↓↓": very significant decrease ($p < 0.01$).

cases. Considering the complexity in 80 year daily simulation and simultaneous multi-gauge optimization at such a large scale, the calibration-validation results can be considered satisfactory for long-term land use/climate change impact assessments according to the evaluation guidelines from SWAT developers (Moriasi et al., 2007, 2015a,b). The model performance shown here is comparable to various other large scale SWAT applications as well (e.g. Abbaspour et al., 2015; Daggupati et al., 2015b, 2016; Faramarzi et al., 2017; Rajib and Merwade, 2017).

5.3. Spatio-temporal dynamics of blue and green water

5.3.1. Sub-basin scale trend analyses

Sub-basin level MK test results provide spatially explicit information on BW-GW dynamics showing their respective trends of change and associated level of significance. Trends in GW are more pronounced because the number of sub-basins showing significant changes in GW trends (Fig. 8) is higher than that for BW trend (Fig. 7). Although Figs. 7 and 8 represent the combined effects of climate and land use, an analogy with Fig. 4 reveals BW being affected more by the changes in precipitation while land use change being more influential on GW. For example, significant changes in GW ($p < 0.01$, either increasing or decreasing) are noticeable in the sub-basins with prominent land use change. Specifically, 35 out of the 43 sub-basins that experienced land use change (Fig. 4) show very significant increasing trends in GW (Fig. 8). For some of the sub-basins in the southern portion of both the middle and upper regions, where no significant land use change has been detected, the decrease in precipitation is likely the main driver for decreasing GW amount. Similarly, significant increasing trend in BW in the northwestern sub-basins (Fig. 7) can be related to the increase in precipitation, because these sub-basins did not experience change in land use. However, both increased precipitation and significant land use change might counteract each other, causing BW to decrease or stay consistent; this is the case for some of the sub-basins in the northeastern part. Overall, increase in precipitation has been contributing to the increasing trend of BW and GW in ORB and vice versa, although the extent of effect on GW trend is nominal; on the contrary, land use change in majority of the sub-basins has been causing GW to increase but BW to decrease.

5.3.2. Regional and basin scale trend analyses

The middle region shows the least change in BW-GW trend (Fig. 9), which can be related to the least impacted land use and precipitation pattern there (Fig. 4; Table 2). Contrary to the other two regions, BW is slightly decreasing in the middle region, follwing the dereasing/unaltered trend of precipitation over 78% of its area. However, land use change over 15% of its area has caused GW to increase, but the trend is statistically insignificant. The lower region shows the most significant change in the trends of both BW and GW in response to the pronounced change in both land use and climate. Similarly, in conjunction with the prominent land use change in the upper region, the GW amount has increased significantly ($p < 0.1$). The upper region also shows an increasing but insignificant trend in BW in response to relatively smaller

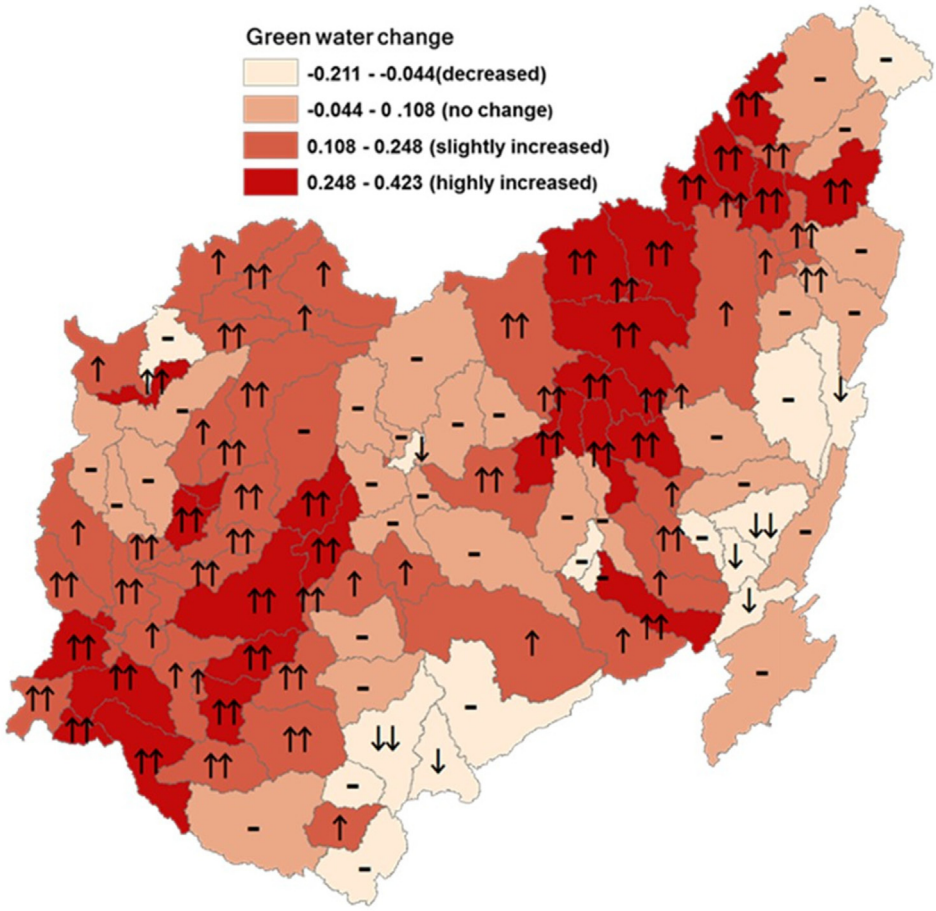

Fig. 8. Sub-basin scale MK trend analysis on green water (GW). Colors and arrows shown in the map hold the same meaning as in Fig. 7 except there is an additional change category (slightly increased and highly increased). Both "slightly" and "highly" increased categories are determined with a threshold of $\tau > 0$.

changes in precipitation amount compared to that in the lower region (Table 2). While land use and climate change have different extent of influence on BW-GW across three regions, the trends in Fig. 10 showing comparatively more significant rate of increase in GW imply equal importance of land use change as a determinant of hydrologic regime for the whole basin and may be the U.S. Midwest in general (e.g. Ahiablame et al., 2017; Rajib and Merwade, 2017). Therefore, studies looking only at climate change would provide partial information which may not be representative of reality.

5.4. Relative effect of climate and land use change

The change in land use has caused more than 70% of the volumetric increment in GW across all three regions (Table 4). Land use change alone has led to decreases in BW by 103% and 42% respectively in the upper and lower regions, but it is the more pronounced effect of climate change (i.e. precipitation, given the context of this study) which has resulted into a net positive change in BW. The relatively consistent climate in the middle region (i.e. unaltered/decreasing precipitation in most parts; Table 2) is responsible for decrease in both BW and GW by 252% and 9% respectively, but the change in land use, though nominal, ultimately resulted into net increase in GW there. These quantitative assessments, coupled with sub-basin/regional/basin-level trend analyses, establish land use change as the controlling factor of GW in ORB; climate change can affect both BW and GW, however, with stronger influence on BW. Therefore, if the hydrologic flux components of BW and GW are analyzed separately, land use change can be found more responsible for changes in ET and root zone soil water (GW), and climate change for water yield and deep aquifer recharge (BW). Although Zhao et al. (2016) obtained nearly similar results showing land use-GW and climate-BW connectivity for another mid-latitude basin in the Asia-Pacific, there is still not enough evidence to apporve this as a generic cause-and-effect relationship.

Some of the previous studies (e.g. Abbaspour et al., 2009; Fu et al., 2007; Jha et al., 2004; Legesse et al., 2003; van Roosmalen et al., 2009) have shown that both temperature and precipitation can be critical on BW-GW; however, these findings are region-specific and may not be analogous to ORB because of the insignificant change in average temperature over the past 80 years (Fig. 3 (c)). Slightly increasing minimum temperature in ORB may still impact hydrologic responses in the northeastern part, more specifically in terms of the volume and timing of snow melt, thereby affecting the seasonal variability of runoff/water yield (e.g. Paul et al., 2017). However, such seasonal aspects have not been analyzed in this study. Gradual lowering of PET limit (Fig. 3(b)) has a decreasing effect on the actual ET (hence, GW) which might have been counteracted by the higher precipitation availability (hence, more water available for ET even under the same PET limit; Paul et al., 2017). Besides these correlated hydro-climatic processes, a "land use – climate circular effect" is possible too. The apparent increase in transpiration from the expanding vegetation, due to re-forestation and agricultural intensification (upper and lower region of ORB, respectively), might have led to cooler day temper-

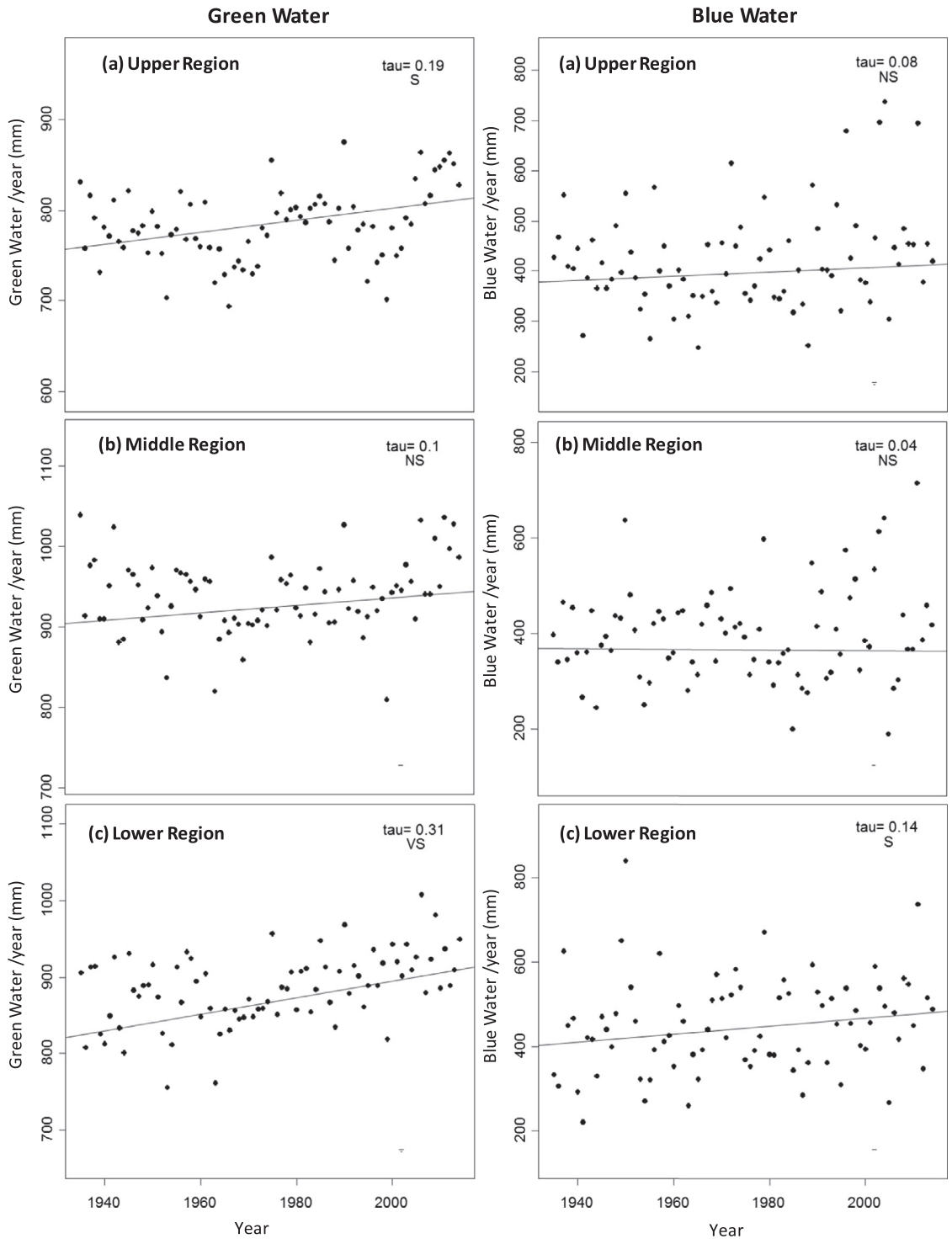

Fig. 9. Mann-Kendall (MK) and Theil-Sen (TS) trend analyses on blue and green water over the (a) the upper region, (b) the middle region and (c) the lower region. Basis for sub-dividing into these three regions is shown in Fig. 4.

ature and subsequent reduction in PET (e.g. Mueller et al., 2016; Fig. 3). Alternatively, a staggering 65 mm increase in GW (i.e. ET and soil water) in 2010s with respect to that in 1940s (Table 4; estimated by the TS trend line) can also be linked with the notable rise of dew point temperature observed across the U.S. Midwest over the last century (Brown and DeGaetano, 2013). Thus, the increased ET in ORB might not be causing the temperature to soar, but it is adding to the humidity, affecting the timing, intensity and spatial pattern of precipitation.

Pertinent to the circular effect between climate and land use/land cover, "CO_2 fertilization" is another important factor that needs attention. It is a well-established fact that atmospheric CO_2 has increased substantially over the past century. With minimal change in vapor pressure deficit (which is likely in ORB as indicated by the trends in temperature and PET; Fig. 3), increase in CO_2 can cause "CO_2 fertilization" by raising the water use efficiency in photosynthesis process (e.g. Donohue et al., 2013; 2017). If there is no change in climate/land use, this "extra efficiency" could

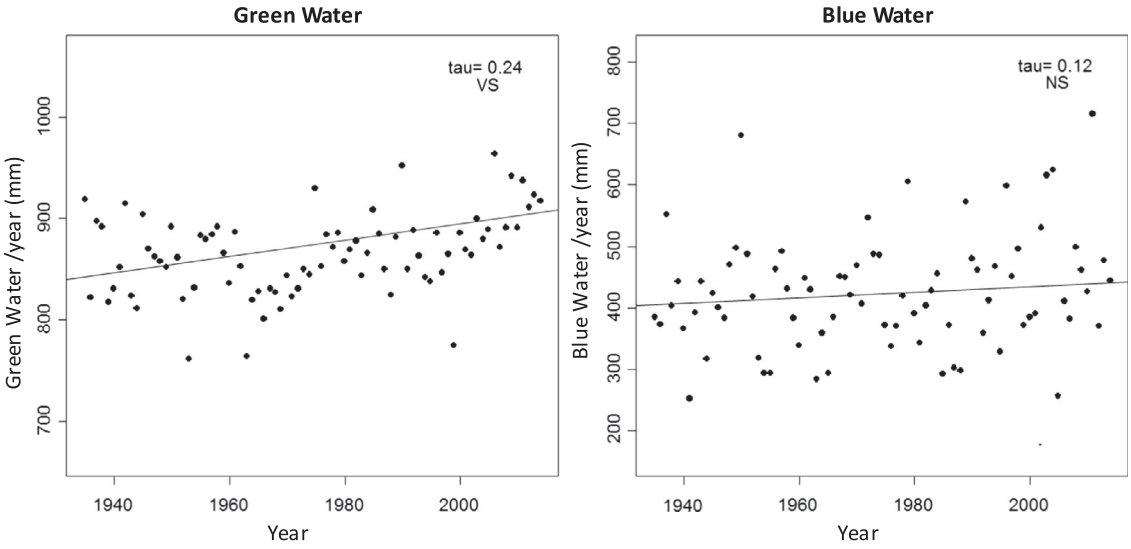

Fig. 10. Mann-Kendall (MK) and Theil-Sen (TS) trend analyses on blue and green water over the entire basin.

Table 4
Volumetric magnitudes and significance of changes in blue water (BW) and green water (GW) at the regional and basin scales, with relative contribution from climate and land use change.[a,b]

		Net change (mm)	Total contribution from climate change only (mm)	% contribution in the net change	
				From climate change	From land use change
Entire Basin	GW	64.5*	6.9	11	89
	BW	35.5	49.4**	139	(−) 39
Upper region	GW	52.2**	7.6	15	85
	BW	33.8	68.6	203	(−) 103
Middle region	GW	36.0	(−) 3.4**	(−) 9	109
	BW	(−) 5.0	(−) 12.6	(−) 252	152
Lower region	GW	85.6*	20.8**	24	76
	BW	75.2**	107.2*	142	(−) 42

[a] * indicates significant at $p < 0.01$, ** indicates significant at $p < 0.1$. Negative sign (−) means that resultant impact leads to a decrease.
[b] Difference between the two end points of a Theil-Sen (TS) slope line, indicating the beginning (1935) and the end (2014) of a time-series, is used as the estimator of change magnitude.

ideally cause photosynthesis to increase while transpiration stays constant or photosynthesis would remain constant while transpiration declines. In ORB, increase in GW outpaced BW in the forested middle/upper regions (Table 4). Thus, a profound indication from this study is that higher precipitation and afforestation have caused increase in the amount of transpiration, while elevated CO_2 concentration might have been enhancing the vegetative productivity in the forests through CO_2 fertilization. This is analogous to the recent findings for tropical forests (Yang et al., 2016) and for many parts of the globe (Zhu et al., 2016). Another important attribute of this vegetation productivity is the increase in root depths in response to elevated CO_2 (Bond and Midgley, 2012; Iversen, 2010), which has profound implication on how vegetation evolves/adapts over time and effects water balance via transpiration. However, changed extent of forested area must not be misinterpreted with the same meaning as the change in vegetative productivity. Although this study has considered varying land use/-climate over the 80 year study period in one of the configurations, all simulations are conducted assuming a constant CO_2 concentration. In this way, SWAT only simulates annual growth cycles of particular vegetation types following an optimal leaf-area development curve, which basically ignores the long-term CO_2 fertilization effect. Such limitation might have imparted some inaccuracies in the results especially in the forested sub-basins.

5.5. Implications of a changing hydrologic regime

Implications of altered BW-GW dynamics span beyond just water availability. For example, increase in BW essentially indicates a directly proportional increase of flooding potential in ORB. This is because, water yield (a component of BW) is simulated as the amount of water leaving the landscape and becoming available in the main channel (water yield = surface runoff + base flow + lateral flow – losses; Neitsch et al., 2011). As deep aquifer recharge (the other component of BW) can only have a trifling change in the 80 year time span, a basin-average 35.5 mm increase of BW in Table 4 essentially mean a ~0.5 mm/year increase in water yield. However, results for the lower region suggest much adverse situation with a statistically significant increasing rate of ~1 mm/year. This means higher expectancy of flooding in the lower region (whole state of Indiana, southeastern part of Illinois and northwestern part of Kentucky) in current times and in near future, even in case of a relatively low-magnitude rainfall event. On the contrary, the middle and upper regions (states of Ohio, West Virginia and Pennsylvania) have relatively timid change in flooding potential as indicated by decreasing/insignificant increasing trends in BW therein (Table 4; Fig. 9). Such spatially explicit attribution of flood hazards supplements the findings from other relevant studies (e.g. Mallakpour and Villarini, 2015). The

increased water yield or BW can also be responsible for higher sediment and nutrient runoff, thus, worsening the surface water quality (Pryor et al., 2014). Local governments would require more investments to prevent increasing threats of contamination and protection of water resources in such contexts.

Change in GW in ORB provides a unique example of human influence on climate change. Due to the elevated ET (i.e. GW) from the increased extent of agriculture and forested landscape respectively in the lower and upper regions, frequent summer droughts are becoming more likely even with precipitation quantity that is slightly less than the average (USEPA, 2016). Accordingly, this might cause reduced crop yield unless additional supply can be allocated for irrigation water. Higher irrigation demand or lower crop yield means more trade-off complexity in the food-energy-water nexus. While these are some of the plausible implications of a changing hydrologic regime that can be inferred from the outcomes of this study, model configurations developed here retain their value to be reused in more exhaustive impact assessments.

5.6. Limitations of the study

The following discussion acknowledges some of the limitations of this study.

1. Use of single HRU for each sub-basin limits finer resolution assessment on local level evolution of hydrologic fluxes. Detailed HRU-scale simulation would cost enormous computational resource and time for such a large scale model.
2. The same spatial coverage of artificial subsurface (tile) drainage and the same draining techniques (depth to drain, spacing etc.) since 1935 are also gross approximations, although effects of tile drainage over the long-term annual volumetric change in BW and GW can be trivial.
3. Land use data for past years have 'agriculture' or 'forest' as generic classes without any spatially explicit detail on crop/plant types. Use of Cropland Data Layer (CDL, https://nassgeodata.gmu.edu/CropScape/) and associated management operations (e.g. timing of crop planting/harvest, fertilization, irrigation etc.) could be an option enabling better representation of soil water and ET by the model (e.g. Faramarzi et al., 2009). However, such data resources for ORB are available only after year 2000.
4. Sub-basin specific CO_2 level during 1935–2014 in the ORB region is not explicitly known. Assumed CO_2 level, spatially constant aerodynamic and canopy resistance terms in PET calculation have imparted some uncertainty in the model.
5. Reservoir operation is not considered due to the lack of storage-release data over the entire 80 year study period.

To mitigate some of these limitations, an uncertainty-informed assessment, showing a prediction-range for the BW-GW outputs (e.g. Faramarzi et al., 2017), could be performed in a future study. Beside precipitation and/or temperature, spatial changes of wind speed, solar radiation and humidity could also be the important indicators of climate change as such their effects on changing hydrologic processes need better understanding. Therefore, additional multi-variate spatial statistical analyses would potentially solidify the findings on changing hydrologic regime.

6. Conclusion

This is the first study on 490,000 km^2 Ohio River Basin (ORB), a significant eco-region in the United States, enabling spatio-temporal characterization of climate and land use change impacts on Blue Water (BW) and Green Water (GW) dynamics. SWAT models are created under two different configurations in order to quantify the combined as well as the relative impacts of climate and land use change in altering the dynamics of BW and GW over an 80 year period (1935–2014). It should be noted that most of the past studies on BW-GW dynamics have assumed constant land use. Although some of the studies have used variable land use in model simulations, the relative influence of climate and land use change on BW-GW dynamics have not been quantified. The current study overcomes these limitations by incorporating representative decadal land use data during 80 years of simulation, and hence, the modeling results are expected to be more representative of the actual hydrologic responses. Based on the statistical trend analyses of modeled outputs at three different spatial scales – the entire basin, 3 sub-regions, and each of the 125 sub-basins, following conclusions can be drawn.

1. Increased precipitation and re-forestation are found as the dominant indicators of climate and land use change in ORB. While changes in precipitation and land use are evident in the upper and lower regions during the 80 years of study, the middle region is relatively least impacted.
2. Between 1935 and 2014, the changing climate and land use have increased both BW and GW across the basin, although change magnitude of GW is twice the magnitude of BW. The lower region exhibits maximum changes where the land use and climate changes have led to significant increasing trends in both BW and GW. Similarly, the GW in upper region has increased significantly in response to land use change. The amount of BW has also increased in the upper region, but the trend is not significant, which corresponds to the relatively smaller changes in precipitation amount in the upper region compared to that in the lower region. The middle region shows the least changes in both BW and GW.
3. Based on the independent contribution of climate and land use, a causal relationship is detected showing that land use change in ORB generally exerts stronger influence on GW dynamics. Climate change affects both BW and GW but the effects are more pronounced on BW.

Overall, this study identifies the *hotspots* within the Ohio River Basin which have been experiencing major changes in BW-GW dynamics in response to climate and land use changes. Sub-basin scale attribution of land use and climate (more specifically, precipitation) change impacts will provide valuable insights to the local stakeholders, whereas regional and basin level assessments will help appropriate decision making on water resources management, protection, and restoration by both the regional watershed managers and the national policy makers. Relative impacts of climate and land use in changing the dynamics of BW and GW, as quantified in this study, will allow adopting mitigation measures in a more efficient and targeted way depending on whether climate change or land use change is the governing factor for a region of interest.

Acknowledgements

Drs. Adnan Rajib and Venkatesh Merwade wrote the paper, while Liuying Du performed modeling and result analyses. This work was partially supported by the National Science Foundation (#OCI-1041379 and #OCI-1148090). Any opinions, findings, and conclusions or recommendations expressed in this material are those of the authors and do not necessarily reflect the views of the National Science Foundation. Authors gratefully acknowledge the constructive suggestions from the reviewers, including those from the Editor-in-Chief Dr. Tim R. McVicar. Authors also thank Kimberly Peterson from the Lyles School of Civil Engineering at the Purdue University for proof-reading the paper.

Appendix A

(see Tables A.1 and A.2)

Table A.1
SWAT calibration parameters.

No.	Parameter[a]	Definition[b]	SWAT file[c]	Initial range
1	v_ALPHA_BF	Baseflow recession constant (days)	.gw	0.01–1
2	v_SURLAG	Surface runoff lag coefficient (days)	.bsn	0.05–24
3	v_CH_K2	Main channel hydraulic conductivity (mm/h)	.rte	5–100
4	v_CH_N2	Main channel Manning's *n*	.rte	0.01–0.15
5	r_CN2	Curve number (moisture condition II)	.mgt	−0.2–0.2
6	v_EPCO	Plant uptake compensation factor	.hru	0–1
7	v_ESCO	Soil evaporation compensation factor	.hru	0–1
8	a_GW_DELAY	Groundwater delay (days)	.gw	−10–10
9	v_GW_REVAP	Groundwater "revap" coefficient	.gw	0.01–0.2
10	v_GWQMN	Threshold depth for return flow (mm H_2O)	.gw	0.01–5000
11	v_REVAPMN	Re-evaporation threshold (mm H_2O)	.gw	0.01–500
12	v_RCHRG_DP	Deep aquifer percolation fraction	.gw	0–1
13	r_SOL_K	Soil saturated hydraulic conductivity (mm/h)	.sol	−0.15–0.15
14	v_SFTMP	Snowfall temperature (°C)	.bsn	0–5
15	v_SMFMN	Melt factor for snow on December 21 (mm H_2O/°C-day)	.bsn	0–10
16	v_SMFMX	Melt factor for snow on June 21 (mm H_2O/°C-day)	.bsn	0–10
17	v_SMTMP	Snow melt base temperature (°C)	.bsn	−2–5
18	v_TIMP	Snow pack temperature lag factor	.bsn	0–1

[a] The indices shown with the parameter names denote the type of change to be applied over the existing parameter value: 'v_' means the original value is to be replaced by a value from the range, 'a_' means a value from the range is added to the original value, 'r_' means the original value is multiplied by the adjustment factor (1+ given value within the range).
[b] Source: Neitsch et al. (2011).
[c] The extension refers to the SWAT file type where the parameters are provided as inputs (.bsn (basin), .hru (Hydrologic Response Units), .rte (main channel; sub-basin level file), .gw (groundwater; HRU level file), .sol (soil/root zone; HRU level file), .mgt (HRU level management file)). Details can be found in Arnold et al. (2012).

Table A.2
Most optimal values (best estimates) of calibrated parameters.[a]

Parameter[b]	Best parameter estimates[c]								
	M1	M2	M3	M4	M5	M6	M7	M8	M9[d]
1. ALPHA_BF	0.74	0.37	0.62	0.37	0.4	0.35	0.41	0.41	0.4
2. SURLAG	11.98	7.52	15.62	7.50	7. 6	7. 9	8. 2	8. 0	7.5
3. CH_K2	84.01	61.91	40.4	62.0	61.1	62.2	64.0	64.8	62.0
4. CH_N2	0.07	0.083	0.076	0.08	0.085	0.079	0.068	0.066	0.084
5. CN2	−0.03	0.005	0.13	0.01	0.004	0.01	−0.001	−0.003	0.006
6. ESCO	0.51	0.9	0.93	0.91	0.89	0.89	0.95	0.95	0.90
7. EPCO	0.28	0.21	0.20	0.21	0.22	0.24	0.17	0.18	0.2
8. GW_DELAY	−3.63	0.95	−1.01	0.96	0.94	0.953	1.1	2.0	1.0
9. GW_REVAP	0.07	0.06	0.074	0.063	0.062	0.065	0.08	0.081	0.063
10. GWQMN	278.0	94.0	1198.0	94.0	94.3	95.0	107.0	110.1	94.0
11. REVAPMN	287.0	303.7	317.7	304.0	301.0	300.0	295.0	289.0	303.7
12. RCHRG_DP	0.34	0.18	0.015	0.175	0.168	0.2	0.15	0.09	0.08
13. SOL_K	0.09	0.02	0.017	0.021	0.02	0.024	0.031	0.02	0.02
14. SFTMP	1.03	1.08	1.98	1.07	1.1	1.2	2.2	1.0	1.07
15. SMFMN	0.35	2.35	1.75	2.35	2.4	2.3	2.35	1.98	2.35
16. SMFMX	8.45	3.25	6.25	3.25	3.3	4.0	4.7	3.9	3.25
17. SMTMP	1.54	1.96	4.33	1.95	1.91	2.0	1.97	1.7	1.96
18. TIMP	0.86	0.97	0.61	0.96	0.965	0.98	0.96	0.91	0.97

[a] After equal number of iterations (1500) in all the cases.
[b] Parameter definitions and their initial ranges are shown in Table A.1.
[c] M1-M8: 8 SWAT models in the 'variable climate-variable land use' configuration. Each of the models is calibrated/validated separately for its respective 10 year simulation period. For example, M1 refers to the model for 1935–1944, M8 refers to 2005–2014 etc.
[d] M9: A single SWAT model for the entire 80 year study period (1935–2014) considering a steady land use since 1940s ('variable climate-steady land use' configuration).

Appendix B

(see Fig. B.1)

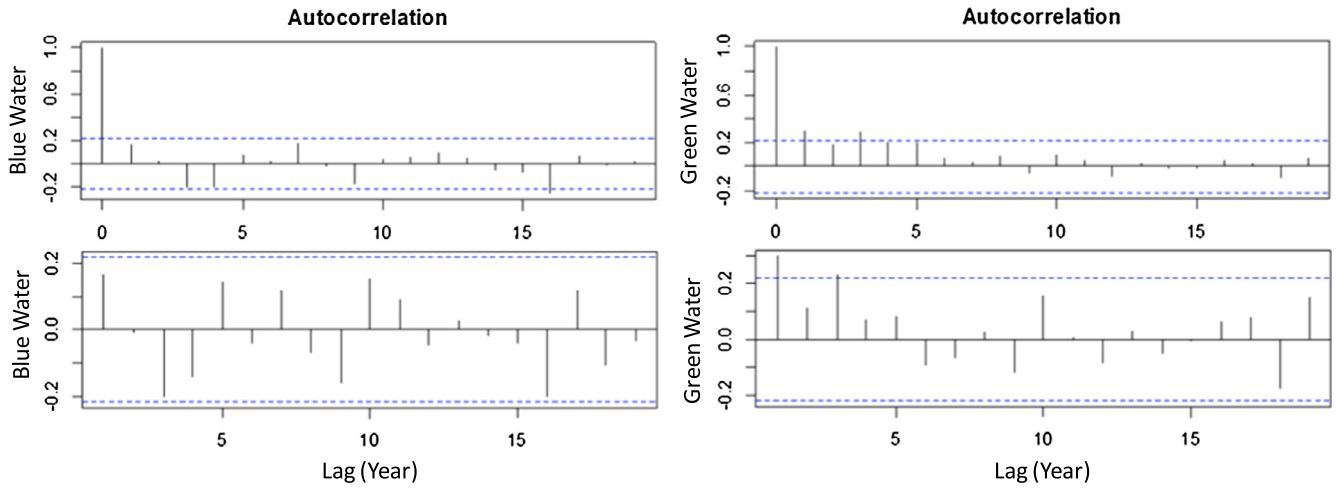

Fig. B.1. Tests of autocorrelation and partial autocorrelation coefficient versus lag time on Blue and Green Water.

References

Abbaspour, K.C., 2015. SWAT-CUP 2012: SWAT calibration and uncertainty programs - a user manual. Available online at: http://swat.tamu.edu/media/114860/usermanual_swatcup.pdf (last cited on March 21, 2016).

Abbaspour, K.C., Rouholahnejad, E., Vaghefi, S., Srinivasan, R., Yang, H., Kløve, B., 2015. A continental-scale hydrology and water quality model for Europe: calibration and uncertainty of a high-resolution large-scale SWAT model. J. Hydrol. 524, 733–752. https://doi.org/10.1016/j.jhydrol.2015.03.027.

Abbaspour, K.C., Faramarzi, M., Ghasemi, S.S., Yang, H., 2009. Assessing the impact of climate change on water resources in Iran. Water Resour. Res. 45, 1–16. https://doi.org/10.1029/2008WR007615.

Ahiablame, L., Sinha, T., Paul, M., Ji, J.-H., Rajib, A., 2017. Streamflow response to potential land use and climate changes in the James River watershed, Upper Midwest United States. J. Hydrol. Regional Studies 14, 150–166. https://doi.org/10.1016/j.ejrh.2017.11.004.

America's Watershed Initiative, 2014. Ohio River Basin. Available online at: http://ian.umces.edu/pdfs/ian_newsletter_434.pdf (last cited on March 18, 2016).

Arnold, J., Moriasi, D., Gassman, P., Abbaspour, K., White, M., Srinivasan, R., Santhi, C., Harmel, R.D., Griensven, A. Van, 2012. SWAT: model use, calibration, and validation. Trans. ASABE 55, 1491–1508.

Boles, C.M.W., Frankenberger, J., Moriasi, D., 2015. Tile drainage simulation in SWAT2012: parameterization and evaluation in an Indiana watershed. Trans. ASABE 58 (5), 1201–1213. https://doi.org/10.13031/trans.58.10589.

Boles, C., 2013. Swat model simulation of bioenergy crop impacts in a tile-drained watershed. MS Thesis, Dept. of Agricultural and Biological Engineering, Purdue University. Available online at: http://docs.lib.purdue.edu/open_access_theses/23 (last cited on July 29, 2016).

Bond, W.J., Midgley, G.F., 2012. Carbon dioxide and the uneasy interactions of trees and savannah grasses. Philos. Trans. R. Soc. London B: Biol. Sci. 367 (1588), 601–612. https://doi.org/10.1098/rstb.2011.0182.

Brown, P.J., DeGaetano, A.T., 2013. Trends in U.S. surface humidity, 1930–2010. J. Appl. Meteorol. Climatol. https://doi.org/10.1175/JAMC-D-12-035.1.

Budyko, M.I., 1974. Climate and Life. Academic Press, p. 508.

Carmona, A.M., Poveda, G., Sivapalan, M., Vallejo-Bernal, S.M., Bustamante, E., 2016. A scaling approach to Budyko's framework and the complementary relationship of evapotranspiration in humid environments: case study of the Amazon River basin. Hydrol. Earth Syst. Sci. 20, 589–603. https://doi.org/10.5194/hess-20-589-2016.

Daggupati, P., Deb, D., Srinivasan, R., Yeganantham, D., Mehta, V.M., Rosenberg, N.J., 2016. Large-scale fine-resolution hydrological modeling using parameter regionalization in the Missouri River Basin. J. Am. Water Resour. Assoc. 52 (3), 648–666. https://doi.org/10.1111/1752-1688.12413.

Daggupati, P., Pai, N., Ale, S., Douglas-Mankin, K.R., Zeckoski, R.W., Jeong, J., Parajuli, P.B., Saraswat, D., Youssef, M.A., 2015a. A recommended calibration and validation strategy for hydrologic and water quality models. Trans. ASABE 58 (6), 1705–1719.

Daggupati, P., Yen, H., White, M.J., Srinivasan, R., Arnold, J.G., Keitzer, C.S., Sowa, S.P., 2015b. Impact of model development, calibration and validation decisions on hydrological simulations in West Lake Erie Basin. Hydrol. Process. 29 (26), 5307–5320. https://doi.org/10.1002/hyp.10536.

Doll, P., Siebert, S., 2002. Global modeling of irrigation water requirements. Water Resour. Res. 38, 1–10. https://doi.org/10.1029/2001WR000355.

Donohue, R.J., Roderick, M.L., McVicar, T.R., Yang, Y., 2017. A simple hypothesis of how leaf and canopy-level transpiration and assimilation respond to elevated CO_2 reveals distinct response patterns between disturbed and undisturbed vegetation. J. Geophys. Res. – Biogeosci. 122 (1), 168–184. https://doi.org/10.1002/2016JG003505.

Donohue, R.J., Roderick, M.L., McVicar, T.R., Farquhar, G.D., 2013. Impact of CO_2 fertilization on maximum foliage cover across the globe's warm, arid environments. Geophys. Res. Lett. 40 (12), 3031–3035. https://doi.org/10.1002/grl.50563.

Donohue, R.J., Roderick, M.L., McVicar, T.R., 2011. Assessing the differences in sensitivities of runoff to changes in climatic conditions across a large basin. J. Hydrol. 406 (3–4), 234–244.

Donohue, R.J., McVicar, T.R., Roderick, M.L., 2010. Assessing the ability of potential evaporation formulations to capture the dynamics in evaporative demand within a changing climate. J. Hydrol. 386 (1–4), 186–197.

Drummond, M.A., Auch, R.F., Karstensen, K.A., Sayler, K.L., Taylor, J.L., Loveland, T.R., 2012. Land change variability and human-environment dynamics in the United States Great Plains. Land Use Policy 29, 710–723. https://doi.org/10.1016/j.landusepol.2011.11.007.

Du, B., Arnold, J., Saleh, A., Jaynes, D., 2005. Development and application of SWAT to landscapes with tiles and potholes. Trans. ASAE 48 (3), 1121–1133.

Eathington, L., 2010. 2000–2009 Population growth in the Midwest: urban and rural dimensions. Department of Economics, Iowa State University. Available online at: www.econ.iastate.edu/sites/default/files/publications/papers/p11427-2010-04-28.pdf (last cited on March 7, 2016).

Falkenmark, M., Rockström, J., 2006. The new blue and green water paradigm: breaking new ground for water resources planning and management. J. Water Resour. Plan. Manage. 132 (3), 129–133. https://doi.org/10.1061/(ASCE)0733-9496(2006) 132:3(129).

Faramarzi, M., Abbaspour, K.C., Schulin, R., Yang, H., 2009. Modelling blue and green water resources availability in Iran. Hydrol. Process. 23. https://doi.org/10.1002/hyp.716.

Faramarzi, M., Abbaspour, K.C., Adamowicz, W.L., Lu, W., Fennell, J., Zehnder, A., Goss, G., 2017. Uncertainty based assessment of dynamic freshwater scarcity in semi-arid watersheds of Alberta. Canada. J. Hydrol Regional Studies 9, 48–68. https://doi.org/10.1016/j.ejrh.2016.11.003.

Fu, G., Charles, S.P., Chiew, F.H.S., 2007. A two-parameter climate elasticity of streamflow index to assess climate change effects on annual streamflow. Water Resour. Res. 43, 1–12. https://doi.org/10.1029/2007WR005890.

Gerten, D., Hoff, H., Bondeau, A., Lucht, W., Smith, P., Zaehle, S., 2005. Contemporary "green" water flows: simulations with a dynamic global vegetation and water balance model. Phys. Chem. Earth 30, 334–338. https://doi.org/10.1016/j.pce.2005.06.002.

Green, C.H., Tomer, M.D., Di Luzio, M., Arnold, J.G., 2006. Hydrologic evaluation of the soil and water assessment tool for a large tile-drained watershed in Iowa. Trans. ASABE 49, 413–422.

Greve, P., Gudmundsson, L., Orlowsky, B., Seneviratne, S.I., 2015. The Budyko framework beyond stationarity. Hydrol. Earth Syst. Sci. Discuss. 12, 6799–6830. https://doi.org/10.5194/hessd-12-6799-2015.

Guo, J., Su, X., Singh, V.P., Jin, J., 2016. Impacts of climate and land use/cover change on streamflow using SWAT and a separation method for the Xiying River Basin in Northwestern China. Water 8. https://doi.org/10.3390/w8050192.

Gupta, H.V., Kling, H., Yilmaz, K.K., Martinez, G.F., 2009. Decomposition of the mean squared error and NSE performance criteria: implications for improving

hydrological modelling. J. Hydrol. 377, 80–91. https://doi.org/10.1016/j.jhydrol.2009.08.003.
Her, Y., Frankenberger, J., Chaubey, I., Srinivasan, R., 2015. Threshold effects in HRU definition of the Soil and Water Assessment Tool. Trans. ASABE 58 (2), 367–378. https://doi.org/10.13031/trans.58.10805.
Hoekstra, A. Y., Hung, P.Q., 2002. Virtual Water Trade: A quantification of virtual water flows between nations in relation to international crop trade, Value of Water Research Report Series No. 11, UNESCO-IHE, Delft, Netherlands. Available online at: http://waterfootprint.org/media/downloads/Report11.pdf (last cited on March 18, 2016).
Hoekstra, A.Y., Chapagain, A.K., Aldaya, M.M., Mekonnen, M.M., 2011. The Water Footprint Assessment Manual: setting the global standard, Earthscan, London, U.K.. Available at: http://waterfootprint.org/media/downloads/TheWaterFootprintAssessmentManual_2.pdf. Accessed March 18, 2016.
Iversen, C.M., 2010. Digging deeper: fine-root responses to rising atmospheric CO2 concentration in forested ecosystems. New Phytol. 186 (2), 346–357. https://doi.org/10.1111/j.1469-8137.2009.03122.x.
Jha, M., Pan, Z., Takle, E.S., Gu, R., 2004. Impacts of climate change on streamflow in the Upper Mississippi River Basin: a regional climate model perspective. J. Geophys. Res. 109, 1–12. https://doi.org/10.1029/2003JD003686.
Jiang, C., Xiong, L., Wang, D., Liu, P., Guo, S., Xu, C.Y., 2015. Separating the impacts of climate change and human activities on runoff using the Budyko-type equations with time-varying parameters. J. Hydrol. 522, 326–338. https://doi.org/10.1016/j.jhydrol.2014.12.060.
Karl, T.R., Knight, R.W., Easterling, D.R., Quayle, R.G., 1996. Indices of climate change for the United States. B. Am. Meteorol. Soc. https://doi.org/10.1175/1520-0477(1996)077<0279:IOCCFT>2.0.CO;2.
Kendall, M.G., 1948. Rank Correlation Methods. Charles Griffin & Co. Ltd..
Kladivko, E., Van Scoyoc, G., Monke, E., Oates, K., Pask, W., 1991. Pesticide and nutrient movement into subsurface tile drains on a silt loam soil in Indiana. J. Environ. Quality 20 (1), 264–270.
Kling, H., Fuchs, M., Paulin, M., 2012. Runoff conditions in the upper Danube basin under an ensemble of climate change scenarios. J. Hydrol. 424–425, 264–277. https://doi.org/10.1016/j.jhydrol.2012.01.011.
Kumar, S., Merwade, V., Kam, J., Thurner, K., 2009. Streamflow trends in Indiana: effects of long term persistence, precipitation and subsurface drains. J. Hydrol. 374, 171–183. https://doi.org/10.1016/j.jhydrol.2009.06.012.
Kunnath-Poovakka, A., Ryu, D., Renzullo, L.J., George, B., 2016. The efficacy of calibrating hydrologic model using remotely sensed evapotranspiration and soil moisture for streamflow prediction. J. Hydrol. 535, 509–524. https://doi.org/10.1016/j.jhydrol.2016.02.018.
Kunkel, K.E., Stevens, L.E., Stevens, S.E., Sun, L., Janssen, E., Wuebbles, D., Hilberg, S. D., Timlin, M.S., Stoecker, L., Westcott, N.E., Dobson, J.G., 2013. Regional climate trends and scenarios for the U.S. National Climate Assessment: Part 3. Climate of the Midwest U.S. NOAA Technical Report NESDIS 142-3. 103 pp., National Oceanic and Atmospheric Administration, National Environmental Satellite, Data, and Information Service, Washington, D.C. Available online at: http://www.nesdis.noaa.gov/technical_reports/NOAA_NESDIS_Tech_Report_142-3-Climate_of_the_Midwest_U.S.pdf. Last cited on July 19, 2016.
Larose, M., Heathman, G.C., Norton, L.D., Engel, B., 2007. Hydrologic and atrazine simulation of the Cedar Creek Watershed using the SWAT model. J. Environ. Qual. 36, 521–531. https://doi.org/10.2134/jeq2006.0154.
Legesse, D., Vallet-Coulomb, C., Gasse, F., 2003. Hydrological response of a catchment to climate and land use changes in Tropical Africa: case study south central Ethiopia. J. Hydrol. 275, 67–85. https://doi.org/10.1016/S0022-1694(03)00019-2.
Li, L., Zhang, L., Xia, J., Gippel, C.J., Wang, R., Zeng, S., 2015. Implications of modelled climate and land cover changes on runoff in the middle route of the South to North Water Transfer Project in China. Water Resour. Manage. 29, 2563–2579. https://doi.org/10.1007/s11269-015-0957-3.
Li, H., Zhang, Y., Vaze, J., Wang, B., 2014. Separating effects of vegetation change and climate variability using hydrological modelling and sensitivity-based approaches. J. Hydrol. 420–421, 403–418. https://doi.org/10.1016/j.jhydrol.2011.12.033.
Li, F., Zhang, G., Xu, Y.J., 2012. Separating the impacts of climate variation and human activities on runoff in the Songhua River Basin, Northeast China. Water 6, 3320–3338. https://doi.org/10.3390/w6113320.
Li, Z., Liu, W., Zhang, X., Zheng, F., 2009. Impacts of land use change and climate variability on hydrology in an agricultural catchment on the Loess Plateau of China. J. Hydrol. 377, 35–42. https://doi.org/10.1016/j.jhydrol.2009.08.007.
Liu, Q., McVicar, T.R., 2012. Assessing climate change induced modification of Penman potential evaporation and runoff sensitivity in a large water-limited basin. J. Hydrol. 464–465, 352–362.
Liu, X., Ren, L., Yuan, F., Singh, V.P., Fang, X., Yu, Z., Zhang, W., 2009. Quantifying the effect of land use and land cover changes on green water and blue water in northern part of China. Hydrol. Earth Syst. Sci. 13, 735–747. https://doi.org/10.5194/hess-13-735-2009.
Lytle, D., 2010. Ohio's statewide forest resource assessment – 2010. Ohio Department of Natural Resources, Division of Forestry. Available at: http://forestry.ohiodnr.gov/portals/forestry/pdfs/FAP/Assessment.pdf. Accessed 15 May, 2017.
Mann, H.B., 1945. Nonparametric tests against trend. Econometrica: J. Econometric Soc., 245-259.
Mallakpour, I., Villarini, G., 2015. The changing nature of flooding across the central United States. Nature Climate Change 5, 250–254. 1038/nclimate2516.
McVicar, T.R., Roderick, M.L., Donohue, R.J., Li, L.T., Van Niel, T.G., Thomas, A., Grieser, J., Jhajharia, D., Himri, Y., Mahowald, N.M., Mescherskaya, A.V., Kruger, A.C., Rehman, S., Dinpashoh, Y., 2012. Global review and synthesis of trends in observed terrestrial near-surface wind speeds: implications for evaporation. J. Hydrol. 416–417, 182–205. https://doi.org/10.1016/j.jhydrol.2011.10.024.
Milly, P.C.D., Dunne, K.A., 2016. Potential evapotranspiration and continental drying. Nature Clim. Change 6 (10), 946–949. https://doi.org/10.1038/nclimate3046.
Moriasi, D.N., Gitau, M.W., Pai, N., Daggupati, P., 2015a. Hydrologic and water quality models: performance measures and evaluation criteria. Trans. ASABE 58 (6), 1763–1785.
Moriasi, D.N., Zeckoski, R.W., Arnold, J.G., Baffaut, C.B., Malone, R.W., Daggupati, P., Guzman, G.A., Saraswat, D., Yuan, Y., Wilson, B.W., Shirmohammadi, A., Douglas-Mankin, K.R., 2015b. Hydrologic and water quality models: key calibration and validation topics. Trans. ASABE 58 (6), 1609–1618. https://doi.org/10.13031/trans.58.11075.
Moriasi, D.N., Arnold, J.G., Van Liew, M.W., Binger, R.L., Harmel, R.D., Veith, T.L., 2007. Model evaluation guidelines for systematic quantification of accuracy in watershed simulations. Trans. ASABE 50, 885–900. https://doi.org/10.13031/2013.23153.
Mueller, N.D., Butler, E., McKinnon, K.A., Rhines, A., Tingley, M., Holbrook, N.M., Huybers, P., 2016. Cooling of US Midwest summer temperature extremes from cropland intensification. Nature Climate Change 6, 317–322. https://doi.org/10.1038/nclimate2825.
Neitsch, S.L., Arnold, J., Kiniry, J., Williams, J., 2011. Soil & Water Assessment Tool theoretical documentation version 2009. Texas A&M University System, College Station, TX, USA.
Neitsch, S.L., Arnold, J.G., Kiniry, J.R., Williams, J.R., 2011. Soil and water assessment tool theoretical documentation version 2009. Texas Water Resources Institute.
Ndomba, P., Mtalo, F., Killingtveit, A., 2008. SWAT model application in a data scarce tropical complex catchment in Tanzania. Phys. Chem. Earth-Parts A/B/C 33, 626–632. https://doi.org/10.1016/j.pce.2008.06.013.
Oeurng, C., Sauvage, S., Sánchez-Pérez, J.-M., 2011. Assessment of hydrology, sediment and particulate organic carbon yield in a large agricultural catchment using the SWAT model. J. Hydrol. 401 (3), 145–153. https://doi.org/10.1016/j.jhydrol.2011.02.017.
Paul, M., Rajib, M.A., Ahiablame, L., 2017. Spatial and temporal evaluation of hydrological response to climate and land use change in three South Dakota watersheds. J. Am. Water Resour. Assoc. 53 (1), 69–88. https://doi.org/10.1111/1752-1688.12483.
Price, K., Purucker, S.T., Kraemer, S.R., Babendreier, J.E., Knightes, C.D., 2014. Comparison of radar and gauge precipitation data in watershed models across varying spatial and temporal scales. Hydrol. Process. n/a–n/a. doi: 10.1002/hyp.9890.
Pryor, S.C., Scavia, D., Downer, C., Gaden, M., Iverson, L., Nordstrom, R., Patz, J., Robertson, G.P., 2014. Ch. 18: Midwest. In J. M. Melillo et al. (Eds.), Climate Change Impacts in the United States: The Third National Climate Assessment, 418-440, US Global Change Research Program. Available online at: http://nca2014.globalchange.gov/report/regions/midwest. Accessed 20 April, 2016.
Pryor, S.C., Barthelmie, R.J., Young, D.T., Takle, E.S., Arritt, R.W., Flory, D., Gutowski, W.J., Nunes, A., Roads, J., 2009. Wind speed trends over the contiguous United States. J. Geophys. Res. 114, D14105. https://doi.org/10.1029/2008JD011416.
Rajib, A., Merwade, V., 2017. Hydrologic response to future land use change in the Upper Mississippi River Basin by the end of 21st century. Hydrol. Process. 31, 3645–3661. https://doi.org/10.1002/hyp.11282.
Rajib, M.A., Merwade, V., 2016. Improving soil moisture accounting and streamflow prediction in SWAT by incorporating a modified time-dependent SCS CN method. Hydrol. Process. 30, 603–624. https://doi.org/10.1002/hyp.10639.
Rajib, M.A., Ahiablame, L., Paul, M., 2016a. Modeling the effects of future land use change on water quality under multiple scenarios: a case study of low-input agriculture with hay/pasture production. Sustainability of Water Quality Ecol. https://doi.org/10.1016/j.swaqe.2016.09.001.
Rajib, M.A., Merwade, V., Yu, Z., 2016b. Multi-objective calibration of a hydrologic model using spatially distributed remotely sensed/in-situ soil moisture. J. Hydrol. 536, 192–207. https://doi.org/10.1016/j.jhydrol.2016.02.037.
Roderick, M.L., Farquhar, G.D., 2011. A simple framework for relating variations in runoff to variations in climatic conditions and catchment properties. Water Resour. Res. 47, 1–11. https://doi.org/10.1029/2010WR009826.
Rodrigues, D.B.B., Gupta, H.V., Mendiondo, E.M., 2014. A blue/green water-based accounting framework for assessment of water security. Water Resour. Res. 50, 7187–7205. https://doi.org/10.1002/2013WR014274.
Rogers, J.C., 2013. The 20th century cooling trend over the southeastern United States. Clim Dyn 40, 341–352. https://doi.org/10.1007/s00382-012-1437-6.
Sadri, S., Kam, J., Sheffield, J., 2016. Nonstationarity of low flows and their timing in the eastern United States. Hydrol. Earth Syst. Sci. 20, 633–649. https://doi.org/10.5194/hess-20-633-2016.
Schilling, K.E., Jha, M.K., Zhang, Y.-K., Gassman, P.W., Wolter, C.F., 2008. Impact of land use and land cover change on the water balance of a large agricultural watershed: Historical effects and future directions. Water Resour. Res. 44, 1–12. https://doi.org/10.1029/2007WR006644.
Schuol, J., Abbaspour, K.C., Yang, H., Srinivasan, R., Zehnder, A.J.B., 2008a. Modeling blue and green water availability in Africa. Water Resour. Res. 44, 1–18. https://doi.org/10.1029/2007WR006609.
Schuol, J., Abbaspour, K.C., Srinivasan, R., Yang, H., 2008b. Estimation of freshwater availability in the West African sub-continent using the SWAT hydrologic model. J. Hydrol. 352 (1), 30–49.

Schnitkey, G., 2013. Concentration of corn and soybean production in the U.S.. Department of Agricultural and Consumer Economics, University of Illinois at Urbana-Champaign. Available online at: http://farmdocdaily.illinois.edu/2013/07/concentration-corn-soybean-production.html (last cited on March 18, 2016).

Sen, P.K., 1968. Estimates of the regression coefficient based on Kendall's tau. J. Am. Stat. Assoc. 63 (324), 1379–1389.

Sleeter, B.M., Sohl, T.L., Loveland, T.R., Auch, R.F., Acevedo, W., Drummond, M.a., Sayler, K.L., Stehman, S.V., 2013. Land-cover change in the conterminous United States from 1973 to 2000. Glob. Environ. Chang. 23, 733–748. https://doi.org/10.1016/j.gloenvcha.2013.03.006.

Sohl, T.L., Sayler, K.L., Bouchard, M., Reker, R.R., Friesz, A.M., Bennett, S.L., Sleeter, B. M., Sleeter, R.R., Wilson, T., Soulard, C., Knuppe, M., Van Hofwegen, T., 2014. Spatially explicit modeling of 1992–2100 land cover and forest stand age for the conterminous United States. Ecol. Appl. 24, 1015–1036. https://doi.org/10.1890/13-1245.1.

Sohl, T.L., Sleeter, B.M., Zhu, Z., Sayler, K.L., Bennett, S., Bouchard, M., Reker, R., Hawbaker, T., Wein, A., Liu, S., Kanengieter, R., Acevedo, W., 2012. A land-use and land-cover modeling strategy to support a national assessment of carbon stocks and fluxes. Appl. Geogr. 34, 111–124. https://doi.org/10.1016/j.apgeog.2011.10.019.

Sugg, Z., 2007. Assessing U.S. farm drainage: Can GIS lead to better estimates of subsurface drainage extent? World Resources Institute. Available online at: http://pdf.wri.org/assessing_farm_drainage.pdf (last cited on August 3, 2017).

Tan, X., Gan, T.Y., 2015. Contribution of human and climate change impacts to changes in streamflow of Canada. Sci. Rep. 5. https://doi.org/10.1038/srep17767.

Tayyebi, A., Pijanowski, B.C., Pekin, B.K., 2015. Land use legacies of the Ohio River Basin: using a spatially explicit land use change model to assess past and future impacts on aquatic resources. Appl. Geogr. 57, 100–111. https://doi.org/10.1016/j.apgeog.2014.12.020.

Tibebe, D., Bewket, W., 2011. Surface runoff and soil erosion estimation using the SWAT model in the Keleta watershed, Ethiopia. Land Degrad. Dev. 22 (6), 551–564.

USDA, 2015. Conservation Fact Sheet. Available at: https://www.fsa.usda.gov/Assets/USDA-FSA-Public/usdafiles/FactSheets/archived-fact-sheets/consv_reserve_program.pdf. Accessed 15 May, 2017.

USEPA, 2016. Climate change indicators in the United States. US Environmental Protection Agency. Available at: https://www.epa.gov/climate-indicators. Accessed 20 April, 2016.

USGS-NED, 2015. National Elevation Dataset: United States Geological Survey National Map Viewer. Available at: http://viewer.nationalmap.gov/viewer/. Accessed 10 March, 2015.

USGS-NLCD, 2016. National Land Cover Database. United States Geological Survey Multi-Resolution Land Characteristics Consortium. Available at: https://www.mrlc.gov/finddata.php. Accessed 15 May, 2016.

USFS, 2009. Ohio forests: 2006. United States Forest Service. Resource bulletin NRS-36. Available at: https://www.nrs.fs.fed.us/pubs/rb/rb_nrs36.pdf. Accessed 15 May, 2017.

van Roosmalen, L., Sonnenborg, T.O., Jensen, K.H., 2009. Impact of climate and land use change on the hydrology of a large-scale agricultural catchment. Water Resour. Res. 45, 1–18. https://doi.org/10.1029/2007WR006760.

von Storch, H., 1999. Misuses of statistical analysis in climate research. In: Analysis of Climate Variability, Springer Berlin Heidelberg.

Wang, D., Hejazi, M., 2011. Quantifying the relative contribution of the climate and direct human impacts on mean annual streamflow in the contiguous United States. Water Resour. Res. 47. https://doi.org/10.1029/2010WR010283.

Wang, D., Tang, Y., 2014. A one-parameter Budyko model for water balance captures emergent behavior in darwinian hydrologic models. Geophys. Res. Lett. 4569–4577. https://doi.org/10.1002/2013GL058740.

White, D., Johnston, K., Miller, M., 2005. Ohio River Basin. In: Benke, A.C., Cushing, C. E. (Eds.), Rivers of North America. Elsevier Academic Press, Burlington, MA, USA.

Wild, M., 2009. Global dimming and brightening: a review. J. Geophys. Res.-Atmos., 114: D00D16. doi: 10.1029/2008JD011470.

Willett, K.M., Jones, P.D., Gillett, N.P., Thorne, P.W., 2008. Recent changes in surface humidity: development of the HadCRUH dataset. J. Climate 21 (20), 5364–5383.

Xu, J., 2013. Effects of climate and land-use change on greenwater variations in the Middle Yellow River, China. Hydrol. Sci. J. 58, 106–117.

Yang, Y., Donohue, R.J., McVicar, T.R., Roderick, M.L., Beck, H.E., 2016. Long-term CO_2 fertilization increases vegetation productivity and has little effect on hydrological partitioning in tropical rainforests. J. Geophys. Res.: Biogeosci. 121, 2125–2140. https://doi.org/10.1002/2016JG003475.

Yue, S., Pilon, P., Phinney, B., Cavadias, G., 2002. The influence of autocorrelation on the ability to detect trend in hydrological series. Hydrol. Process. 16, 1807–1829. https://doi.org/10.1002/hyp.1095.

Zang, C., Liu, J., 2013. Trend analysis for the flows of green and blue water in the Heihe River basin, northwestern China. J. Hydrol. 502, 27–36. https://doi.org/10.1016/j.jhydrol.2013.08.022.

Zang, C.F., Liu, J., Van Der Velde, M., Kraxner, F., 2012. Assessment of spatial and temporal patterns of green and blue water flows under natural conditions in inland river basins in Northwest China. Hydrol. Earth Syst. Sci. 16, 2859–2870. https://doi.org/10.5194/hess-16-2859-2012.

Zhang, Y.K., Schilling, K.E., 2006. Increasing streamflow and baseflow in Mississippi River since the 1940 s: effect of land use change. J. Hydrol. 324, 412–422. https://doi.org/10.1016/j.jhydrol.2005.09.033.

Zhao, A., Zhu, X., Liu, X., Pan, Y., Zuo, D., 2016. Impacts of land use change and climate variability on green and blue water resources in the Weihe River Basin of northwest China. Catena 137, 318–327. https://doi.org/10.1016/j.catena.2015.09.018.

Zhu, Z. et al., 2016. Greening of the Earth and its drivers. Nature Clim. Change 6 (8), 791–795. https://doi.org/10.1038/nclimate3004.

Zucker, L.A., Brown, L.C., 1998. Agricultural drainage: Water quality impacts and subsurface drainage studies in the Midwest. Ohio State University Extension Bulletin 871. The Ohio State University.